

1 **Quantifying the correlation between mobile continents**
2 **and elevated temperatures in the subcontinental mantle**

3 **C. Jain, A. B. Rozel, P. J. Tackley**

4 Institute of Geophysics, Department of Earth Sciences, ETH Zurich, Sonneggstrasse 5, CH-8092 Zurich,
5 Switzerland

6 **Key Points:**

- 7 • Correlation decreases with increasing core temperature, number of continents, in-
8 ternal heating, or decreasing reference viscosity
- 9 • Downwellings along continental margins increase thermal contrast between sub-
10 continental and suboceanic mantle
- 11 • Decompression melting leads to basaltic crust production which breaks the con-
12 tinents and destroys the correlation

Corresponding author: C. Jain, charitra1989@gmail.com

Abstract

Continents influence the mantle’s convective wavelength and the heat flow escaping from the planet’s surface. Over the last few decades, many numerical and analytical studies have contributed to the debate about whether the continents can warm up the subcontinental mantle or not and if they do, then to what extent? However, a consensus regarding the exact nature and magnitude of this correlation between continents and elevated temperatures in the subcontinental mantle remains to be achieved. By conducting a systematic parameter study using 2D global mantle convection simulations with mobile continents, we provide qualitative and quantitative observations on the nature of this correlation. In our incompressible and compressible convection models, we observe the general processes of downwellings bringing cold material into the mantle along continental margins and a subsequent buildup of warm thermal anomalies underneath the continents. We compute the amplitude and degree of this correlation using spectral decomposition of the temperature and composition fields. The dominant degree of correlation evolves with time and changes with continental configuration. Using simple empirical fits, we observe that this correlation decreases with increasing core temperature, number of continents, internal heating, or decreasing reference viscosity. We also report simple regressions of the time-dependence of this correlation. Additionally, we show that decompression melting as a result of a mantle upwelling or small-scale sublithospheric convection leads to voluminous volcanism. The emplacement of this dense basalt-eclogite material breaks the continents apart and destroys the correlation.

1 Introduction

The existence of dynamic feedback between the convecting mantle and the drifting continents is evident from numerical simulations and laboratory experiments. It has been shown that continents exert a first-order influence on Earth’s mantle flow by affecting convective wavelength and surface heat flow (e.g., Grigné, Labrosse, & Tackley, 2007; Guillou & Jaupart, 1995; Gurnis, 1988; Lowman & Gable, 1999; Lowman & Jarvis, 1993, 1996; B. Phillips & Bunge, 2005; Yoshida, Iwase, & Honda, 1999; S. Zhong & Gurnis, 1993; S. Zhong & Liu, 2016; S. Zhong, Zhang, Li, & Roberts, 2007). The notion that continents can have an insulating effect on the mantle has received considerable attention over the last few decades (Cooper, Lenardic, & Moresi, 2006; Cooper, Moresi, & Lenardic, 2013; Lenardic & Moresi, 2001; Lenardic, Moresi, Jellinek, & Manga, 2005).

Numerical simulations by Gurnis (1988); S. Zhong and Gurnis (1993) showed the accumulation of heat underneath mechanically stiff, thick continental plates, and the development of long-wavelength thermal structures in the mantle. By using laboratory experiments, Guillou and Jaupart (1995) proposed that continents wider than the mantle depth are susceptible to breakup as they generate large positive thermal anomalies below them. Lowman and Gable (1999) suggested that the inclusion of oceanic plates and internal heating in convection modeling reduces the thermal contrast between suboceanic and subcontinental mantle. By modeling mechanically and thermally distinct continental and oceanic plates, but with the same thickness and a depth-dependent viscosity, Heron and Lowman (2010, 2011) argued that continental insulation plays a minor role in affecting the mantle’s thermal field and did not report any elevated temperatures in the subcontinental mantle on timescales relevant to supercontinent assembly. Heron and Lowman (2014) further highlighted the decreasing influence of continental insulation on subcontinental mantle temperatures with increasing Rayleigh number Ra , albeit with a stationary supercontinent and viscosity not being fully temperature-dependent in their models. In their mixed-heating (basal and internal) cartesian models, O’Neill, Lenardic, Jellinek, and Moresi (2009) showed the propensity of plumes to rise underneath continents (~ 3000 km in extent) and elevate temperatures away from the cold slabs subducting along continental margins. This temperature anomaly diminishes with strongly temperature dependent viscosity. Moreover, for continents over 8000 km in width, the

65 inefficient lateral advection of material underneath the continents results in the forma-
66 tion of drip instabilities causing small-scale convection cells and a reduction in the ther-
67 mal anomaly. They also explored the possible relation between melting and rifting and
68 did not observe voluminous volcanism owing to hot upwelling subcontinental mantle in
69 their steady-state simulations. By simulating mobile continents, B. R. Phillips and Coltice
70 (2010) also observed an increase in subcontinental temperature as a function of both con-
71 tinental extent and convective wavelength, although their models lacked oceanic plates
72 and a temperature-dependent viscosity, which might result in overestimation of the re-
73 sulting temperature difference between suboceanic and subcontinental mantle. Based on
74 their purely internally heated 3D models with various continental configurations and width,
75 Rolf, Coltice, and Tackley (2012) showed temperature excess of up to 140 K underneath
76 the continents compared to the suboceanic mantle. They showed that as opposed to a
77 dispersed configuration, a cluster of continents results in higher insulation and provides
78 a possible explanation for the episodic continental crustal growth (Condie, 2004; Hawkesworth
79 & Kemp, 2006; Pearson, Parman, & Nowell, 2007). The absence of basal heating and
80 plumes in their models is a significant simplification and demands further testing.

81 Considering all these numerical studies with varying degrees of complexity, some
82 underlying processes have been agreed upon. First, subcontinental mantle can become
83 hotter than suboceanic mantle provided that subduction zones develop along continen-
84 tal margins and inhibit lateral mantle flow. Furthermore for this transient thermal anomaly
85 to develop, the continents would have to be stationary for a sufficient length of time. Sec-
86 ond, any factors that promote thermal mixing will diminish the amplitude of these anom-
87 alies. Most of these studies have however neglected the effects of melting-induced crustal
88 production (hereafter, referred to as MCP) which are considered as significant processes
89 in planetary evolution and dynamics (e.g., Davies, 2007; Nakagawa & Tackley, 2012; Ogawa,
90 2014; Stevenson, 1990; Xie & Tackley, 2004b). Lourenço, Rozel, and Tackley (2016) have
91 also shown that MCP strongly enhances the mobility of the lid and extends the range
92 of parameters over which a mobile lid is present on planets. Aiming for more realistic
93 simulations, we consider MCP in a subset of our simulations.

94 Understanding the mechanism behind the voluminous magmatism and the result-
95 ing formation of continental flood basalts (CFB) remains a contentious issue. Anderson
96 (1982) proposed that the geoid highs above Africa and South Pacific were caused by el-
97 evated temperatures generated by the assembly of the Pangea supercontinent during the
98 Mesozoic. Coltice et al. (2009); Coltice, Phillips, Bertrand, Ricard, and Rey (2007) ar-
99 gued in favor of continental-aggregation induced elevated temperatures and large-scale
100 melting that caused the emplacement of continental flood basalts of the Central Atlantic
101 Magmatic Province following the breakup of Pangea. Alternatively, it has been proposed
102 that deep-seated mantle plumes can cause intense magmatic activity while emplacing
103 continental flood basalts followed by continental breakup (Campbell & Griffiths, 1990;
104 Condie, 2004; Morgan, 1972; Richards, Duncan, & Courtillot, 1989; Scrutton, 1973; White
105 & McKenzie, 1989).

106 In this paper, we study the possible correlation between mobile continents and el-
107 evated subcontinental mantle temperatures using a broad range of thermo-chemical man-
108 tle convection simulations. We systematically vary parameters such as core-mantle bound-
109 ary (CMB) temperature, continental configuration, mantle heating modes (internal and
110 basal heating), and reference viscosity. We further investigate the effect of MCP on this
111 correlation and explore the possible origin of continental flood basalts. We introduce the
112 methodology and the governing equations in section 2. We present the results of our sim-
113 ulations in section 3 and discuss their geophysical implications in section 4. Finally, we
114 summarize the key aspects of our study in section 5.

2 Physical Model and Numerical Model

We study the thermo-chemical evolution of the mantle coupled with mobile continents. Continents are simplified as homogeneous Archean cratons and represented by a continuous non-diffusive compositional field C ($0 \leq C \leq 1$) ($C = 1$ being pure continental and $C = 0$ being pure non-continental material). In our models, these different cratons are allowed to drift closer and collide. They can then drift as a combined continent or move apart. We do not specify a distinct continental thermal conductivity. Compared to the ephemeral oceanic crust that reaches a maximum age of ~ 200 Myr, continents are much older (Rudnick & Gao, 2003). Geophysical, geochemical, and geological investigations have attributed continents' long-term stable behavior to the presence of strong, compositionally buoyant, and possibly viscous cratonic roots underlying the continental crust (Boyd, 1987, 1989; Hirth & Kohlstedt, 1996; Jordan, 1978, 1979; Lee, 2003; Pollack, 1986; Schutt & Leshner, 2006). Accordingly, continents are modeled as lighter and more viscous than the mantle. We use models featuring both incompressibility (with non-dimensional units) and compressibility (with dimensional units) with parameters listed in Table 1. The numerical model employed here incorporates pressure-temperature-dependence of viscosity, internal and basal heating, plasticity, phase transitions, diffusion creep, melting, and crustal production and is an extension of the ones described by Rolf et al. (2012); Rolf and Tackley (2011).

2.1 Rheology

In our models, diffusion creep with homogenous grain size is the viscous deformation mechanism. Between continents and mantle material, the density contrast is specified by the buoyancy ratio B and the rheological contrast is controlled by viscosity ratio $\Delta\eta^C$ and yield stress ratio $\Delta\tau_Y^C$. The mantle is divided into 3 different layers i : upper mantle (1), lower mantle (2) and post-perovskite layer (3), with each layer having different values for activation energy E_i and activation volume V_i (Karato & Wu, 1993; Yamazaki & Karato, 2001). See Table 2 for a list of the rheological properties used in the study. The dimensional temperature-, pressure- and composition-dependent viscosity η in each layer i is given by an Arrhenius law:

$$\eta(T, P, C) = \eta_0 \Delta\eta_i \Delta\eta^C \exp\left(\frac{E_i + PV_i}{RT} - \frac{E_i}{RT_0}\right), \quad (1)$$

where η_0 is the reference viscosity at zero pressure and reference temperature T_0 (1600 K), $\Delta\eta_i$ is the viscosity offset between layer i and the reference viscosity, P is the pressure, R is the gas constant and T is the dimensional absolute temperature. η_0 is valid for the phase system olivine and the reference composition (60% olivine and 40% pyroxene-garnet), both of which have viscosity multipliers of 1 (see Table 2).

Following the viscosity profile expected by the inversion of postglacial rebound data (Čížková, van den Berg, Spakman, & Matyska, 2012) and geoid inversion studies (e.g., Ricard, Richards, Lithgow-Bertelloni, & Le Stunff, 1993; Ricard, Vigny, & Froidevaux, 1989), a viscosity jump of 30 is applied at the upper-lower mantle transition (660 km). As suggested by mineral physics experiments and theoretical calculations (Ammann, Brodholt, Wookey, & Dobson, 2010; Hunt et al., 2009), an additional viscosity jump of 0.1 (compared to reference viscosity) is imposed at the transition to post-perovskite at lowermost mantle depths (2740 km). The activation volume decreases exponentially with increasing pressure in each layer i according to the relation:

$$V(P) = V_i \exp\left(-\frac{P}{P_i}\right). \quad (2)$$

where P_i is the pressure scale which is different for each layer i as given in Table 2.

159 In simulations featuring incompressibility (non-dimensional units), the viscosity takes
 160 the form:

$$\eta(T^*, C) = \Delta\eta^C \exp\left(\frac{\tilde{E}_A}{T^* + 1} - \frac{\tilde{E}_A}{2}\right), \quad (3)$$

161 where $\Delta\eta^C = \eta(T^*, C = 1) / \eta(T^*, C = 0)$ accounts for the compositional depen-
 162 dence, and $\tilde{E}_A = 2 \ln(\eta(T^* = 0, C) / \eta(T^* = 1, C))$ is the non-dimensional activation
 163 energy, which accounts for the temperature-dependence of the viscosity. A constant value
 164 of 23.03 for \tilde{E}_A gives five orders of magnitude viscosity variation in the interval of non-
 165 dimensional temperature $0 \leq T^* \leq 1$. By adding an offset to the temperature, Eq. 3
 166 is obtained from Eq. 1 using the relation:

$$\frac{E}{RT} = \frac{E}{R(T_{\text{surf}} + \Delta T T^*)} = \frac{E}{RT_{\text{surf}}} \frac{1}{(1 + \Delta T/T_{\text{surf}} T^*)} = \frac{\tilde{E}_A}{1 + T^*}, \quad (4)$$

167 where T_{surf} is the surface temperature and ΔT is the temperature scale. In our
 168 case, as is often done in geodynamics, we simply considered that $T_{\text{surf}} = \Delta T$ and the
 169 non-dimensional activation energy is defined by $\tilde{E}_A = E / (RT_{\text{surf}})$. This approxima-
 170 tion might seem quite strong but what matters is the viscosity contrast more than the
 171 exact shape of the viscosity profile.

172 To break the stagnant lid and obtain Earth-like plate tectonics, plastic yielding is
 173 assumed to be the weakening mechanism (Moresi & Solomatov, 1998; Tackley, 2008b).
 174 The maximum stress that a material can sustain before deforming plastically is given
 175 by the yield stress τ_Y and it increases linearly with depth d at a rate of τ'_Y ,

$$\tau_Y(d, C) = \Delta\tau_Y^C \left(\tau_Y^0 + d\tau'_Y\right), \quad (5)$$

176 where $\Delta\tau_Y^C = \tau_Y(d, C = 1) / \tau_Y(d, C = 0)$ accounts for the different yield stresses
 177 of continental and oceanic lithosphere. $\tau_Y^0 = \tau_Y(d = 0, C = 0)$ is the yield stress at the
 178 oceanic surface. If the convective stresses exceed the yield stress, the viscosity is reduced
 179 to the yielding viscosity $\eta_Y = \tau_Y / 2\dot{\epsilon}$, where $\dot{\epsilon}$ is the 2nd invariant of the strain-rate ten-
 180 sor. The effective viscosity is then given by:

$$\eta_{\text{eff}} = \left(\frac{1}{\eta} + \frac{2\dot{\epsilon}}{\tau_Y}\right)^{-1}. \quad (6)$$

181 In simulations with MCP, the viscosity is limited between 10^{18} and 10^{25} Pa·s to mit-
 182 igate large viscosity variations, which would decrease the stability of the code. These vis-
 183 cosity cutoffs are reached at temperatures of ~ 1150 K (highest viscosity) and ~ 5900 K
 184 (lowest viscosity). We therefore resolve the viscosity of the mantle through the entire evo-
 185 lution of the Earth.

186 Continents are less dense by $\Delta\rho_{\text{craton}} = -100$ kg/m³ (buoyancy ratio $B = \Delta\rho_{\text{craton}} / (\alpha\rho_0\Delta T)$)
 187 = -0.4 with thermal expansivity α , reference density ρ_0 and temperature scale ΔT) com-
 188 pared to the mantle. A viscosity ratio $\Delta\eta^C = 100$ and yield stress ratio $\Delta\tau_Y^C = 10$
 189 are used to ensure cratonic lithosphere's relative stability and longevity when compared
 190 to oceanic lithosphere. When considering non-dimensional units, yield stresses τ_Y are
 191 non-dimensionalized with the factor $\eta_0\kappa/D^2$. The dimensional time t is obtained from
 192 the dimensionless time t^* using $t = t^*D^2/\kappa$ and similarly, velocities v are obtained from
 193 dimensionless velocities v^* using $v = v^*\kappa/D$.

208 **Table 1.** Non-dimensional and dimensional parameters used in this study. Parameters that
 209 vary with simulations are given in Table 4.

Property	Symbol	Value	Units
Comp. yield stress ratio	$\Delta\tau_Y^C$	10	-
Comp. viscosity ratio	$\Delta\eta^C$	100	-
Reference density	ρ_0	3300	kg/m ³
Density contrast	$\Delta\rho_{\text{craton}}$	-100	kg/m ³
Surface temperature	T_{surf}	300	K
Specific heat capacity	C_P	1200	J/kg/K
Gas constant	R	8.3145	J/K/mol
Gravity	g	9.81	m/s ²
Mantle thickness	D	2890	km
Surface thermal expansivity ^s	α	$3 \cdot 10^{-5}$	K ⁻¹
Surface thermal diffusivity ^s	κ	$7.57 \cdot 10^{-7}$	m ² /s
Incompressible convection			
Surface yield stress	τ_Y^0	37	MPa
Initial potential temperature	$T_{\text{P}0}$	1550	K
Surface thermal conductivity ^s	k	3.0	W/m/K
Compressible convection with MCP			
Surface yield stress	τ_Y^0	40	MPa
Yield stress gradient	τ_Y'	0.005	-
Initial potential temperature	$T_{\text{P}0}$	1900	K
Surface thermal conductivity ^s	k	3.5	W/m/K
Reference viscosity	η_0	$1 \cdot 10^{20}$	Pa·s
Latent heat of melting	L	600	kJ/kg

^s valid at the surface for olivine phase system.

194 The potential correlation between continents and temperature in the subcontinental
 195 mantle is strongly related to mantle stirring. However, as we use different values of
 196 reference viscosity in models with incompressibility, the average number of overturns occurring
 197 in the mantle decreases for cases with higher viscosity for a given amount of dimensional
 198 time. To overcome this issue, we use a renormalized time t_{r} based on the average
 199 dimensional velocity of our simulations. The renormalized time is given by:

$$t_{\text{r}} = \frac{v_{\text{E}}}{\langle v \rangle_t} t, \quad (7)$$

200 with

$$\langle v \rangle_t = \frac{1}{t_{\text{max}}^*} \int_{t^*=0}^{t^*=t_{\text{max}}^*} v_{\text{RMS}} dt^*, \quad (8)$$

201 where v_{RMS} is the dimensional root-mean-square (RMS) velocity in the whole domain
 202 and v_{E} is the average plate velocity for present-day Earth (3.4 cm/yr as used in
 203 Coltice, Rolf, Tackley, and Labrosse (2012) considering a transit time of 85 Myr for present-day
 204 Earth's mantle). t_{max}^* is the final dimensionless time in our simulations. We thus
 205 force a sufficiently large number of overturns in all cases, which leads to comparable evolution
 206 states. This renormalization is not required for models with compressibility and
 207 dimensional units.

210 **Table 2.** Rheological properties used for compressible convection in 3 different layers i .

Property	Symbol	Value	Units
- Upper Mantle (Olivine)			
Activation energy	E_1	300	kJ/mol
Activation volume	V_1	5.00	cm ³ /mol
Pressure scale	P_1	∞	GPa
Viscosity multiplier	$\Delta\eta_1$	1.0	-
- Lower Mantle (Perovskite)			
Activation energy	E_2	370	kJ/mol
Activation volume	V_2	3.65	cm ³ /mol
Pressure scale	P_2	200	GPa
Viscosity multiplier	$\Delta\eta_2$	30.0	-
- Post-perovskite layer			
Activation energy	E_3	162	kJ/mol
Activation volume	V_3	1.40	cm ³ /mol
Pressure scale	P_3	1610	GPa
Viscosity multiplier	$\Delta\eta_3$	0.1	-

211 **2.2 Conservation Equations, Boundary Conditions and Solution Method**

212 Using the code StagYY (Tackley, 2008a), we solve the equations for both incom-
 213 pressible (Boussinesq approximation) and compressible (anelastic approximation with
 214 infinite Prandtl number) Stokes flow. The equations of conservation of mass, momen-
 215 tum, and energy governing compressible flow are (see (Chandrasekhar, 1961; Schubert,
 216 Turcotte, & Olson, 2001) for details):

$$\frac{\partial}{\partial x_j} (\rho v_j) = 0, \quad (9)$$

$$0 = -\frac{\partial P}{\partial x_i} + \frac{\partial}{\partial x_j} \left\{ \eta \left(\frac{\partial v_i}{\partial x_j} + \frac{\partial v_j}{\partial x_i} - \frac{2}{3} \delta_{ij} \frac{\partial v_k}{\partial x_k} \right) \right\} + \rho g_i, \quad (10)$$

$$\rho C_P \left(\frac{\partial T}{\partial t} + \mathbf{v} \cdot \nabla T \right) - \alpha T (v_r \cdot \nabla_r P) = \nabla \cdot (k \nabla T) + \frac{\partial v_i}{\partial x_j} \sigma_{ij} + \rho H, \quad (11)$$

217 with density ρ , position x_j ($j = 1, 2, 3$ hereinafter), velocity component v_j , Kronecker
 218 delta δ_{ij} , gravity g , specific heat capacity C_P , thermal expansivity α , thermal conduc-
 219 tivity k , stress tensor σ_{ij} and internal heating rate per unit mass H (when specified).
 220 The reader is referred to Rolf et al. (2012) for equations describing incompressible flow.

221 We use a 2D spherical annulus geometry (Hernlund & Tackley, 2008) with a vary-
 222 ing radial resolution and the domain is discretized by 768 (lateral) times 64 (radial) cells.
 223 4,915,200 tracers are advected through the domain using a 4th-order Runge-Kutta method,
 224 and converted to a continuum compositional field using the tracer-ratio method (Tack-
 225 ley & King, 2003) (983,040 tracers in compressible convection calculations). This rep-
 226 resents an average of 100 tracers per cell for the incompressible convection simulations
 227 and 20 tracers per cell for the simulations considering compressibility and MCP. How-
 228 ever, in the latter case, the surface cells are typically replenished with tracers due to mag-
 229 matism, which results in a local increase of tracer density. We employ free-slip bound-

251 **Table 3.** Phase change parameters for Olivine and Pyroxene-Garnet phase systems. ρ_S is the
 252 surface density at zero pressure, $\Delta\rho$ is the density jump across a phase transition, and γ is the
 253 Clapeyron slope.

Depth (km)	Temperature (K)	$\Delta\rho$ (kg/m ³)	γ (MPa/K)
Olivine ($\rho_S = 3240$ kg/m ³)			
410	1600	180	2.5
660	1900	400	-2.5
2740	2300	61.6	10
Pyroxene-Garnet ($\rho_S = 3080$ kg/m ³)			
60	1000	350	0
400	1600	150	1
720	1900	400	1
2740	2300	61.6	10

230 ary conditions for the surface and the core-mantle boundary with the surface temper-
 231 ature fixed as 300 K. In models featuring compressibility, core cooling is included with
 232 a parameterization based on (Buffett, Huppert, Lister, & Woods, 1992, 1996) and for
 233 the parameterization details, the reader is referred to (Nakagawa & Tackley, 2004). The
 234 code uses a finite volume discretization, with velocity and pressure defined on a staggered
 235 grid. For incompressible convection calculations, a multigrid solver is used. For compress-
 236 ible convection calculations, a parallel MUMPS solver from the PETSc package is used
 237 (Amestoy, Duff, & L'Excellent, 2000).

238 2.3 Phase Changes and Composition

239 The model includes a parameterization based on mineral physics data (Irifune &
 240 Ringwood, 1993; Ono, Ito, & Katsura, 2001) in which minerals are divided into olivine
 241 and pyroxene-garnet systems that undergo solid-solid phase transitions, as used in pre-
 242 vious studies (Nakagawa & Tackley, 2012; Xie & Tackley, 2004b). Their mixture depends
 243 on the chemical composition, which varies between basalt (100% pyroxene-garnet) and
 244 harzburgite (75% olivine and 25% pyroxene-garnet). The mantle is initialized with a py-
 245 rolytic composition, which is taken as a petrological mixture of 80% harzburgite and 20%
 246 basalt (e.g. as in Xu, Lithgow-Bertelloni, Stixrude, and Ritsema (2008)). The phase change
 247 parameters are given in Table 3. At a depth of 60 km, basalt forms eclogite, which is around
 248 190 kg/m³ denser than olivine. At lowermost mantle depths, the phase transition from
 249 perovskite to post-perovskite is also considered (e.g., Tackley, Ammann, Brodholt, Dob-
 250 son, & Valencia, 2013).

254 2.4 Melting and Crustal Production

255 When melting is considered, melt-induced differentiation changes the composition
 256 following previous work by Lourenço et al. (2016); Nakagawa, Tackley, Deschamps, and
 257 Connolly (2010); Xie and Tackley (2004b). The composition and temperature fields are
 258 stored and advected on tracers. As melting is calculated on a cell level to ensure numer-
 259 ical efficiency, the cell-based solid composition and melt fraction are computed at cell
 260 centers using mass averaging of these tracers. At each time-step, the required change in
 261 melt fraction for every cell is computed by comparing cell temperature T_{cell} with the
 262 composition-dependent pyrolite solidus T_{sol} (as used by Nakagawa and Tackley (2004)).
 263 The solidus temperature is a function fitting experimental data by Herzberg, Ratteron,

264 and Zhang (2000) in the upper mantle and by Zerr, Diegeler, and Boehler (1998) in the
 265 lower mantle, which is increased linearly by up to 60 K as the basaltic component is de-
 266 pleted, with no melting possible once the basaltic component has been completely re-
 267 moved. In case the cell temperature exceeds or is lower than the solidus, then either more
 268 melt is generated or the existing melt is frozen in the cell to bring the cell temperature
 269 back to the solidus. Latent heat of melt is consumed during melting and released dur-
 270 ing freezing and the resulting change in temperature ΔT_{cell} is computed for each cell.
 271 Accordingly, molten basaltic tracers are created in each cell. If the melt generated on
 272 tracers is at less than 300 km depth, it is instantaneously removed and erupted at the
 273 surface by transporting the tracers. The erupted melt is further solidified to generate
 274 oceanic crust with the surface temperature (Christensen & Hofmann, 1994; Xie & Tack-
 275 ley, 2004a). This is equivalent to considering a much shorter time-scale of melt migra-
 276 tion than that of the mantle flow (Kelemen, Hirth, Shimizu, Spiegelman, & Dick, 1997).

277 2.5 Criterion for Correlation

278 To investigate whether there is a correlation between continents and elevated tem-
 279 peratures in the subcontinental mantle, we perform Fourier decompositions of both tem-
 280 perature T and composition C fields. The Fourier coefficients $a_{l,f}, b_{l,f}$ of field f for har-
 281 monic degree l are given by:

$$a_{l,f} = \frac{1}{\pi(d_2 - d_1)} \int_{\theta=0}^{2\pi} \int_{d_1}^{d_2} f(\theta, R) \cos(l\theta) dR d\theta, \quad (12)$$

$$b_{l,f} = \frac{1}{\pi(d_2 - d_1)} \int_{\theta=0}^{2\pi} \int_{d_1}^{d_2} f(\theta, R) \sin(l\theta) dR d\theta, \quad (13)$$

282 where d_1 and d_2 are the heights (measured from the base of the mantle) between which
 283 the temperature and composition fields are averaged. For the composition field, the Fourier
 284 coefficients are obtained by averaging in the top 100 km of the mantle: $d_2 - d_1 = 2890 -$
 285 $2790 = 100$ km. The spectral decomposition of the temperature field is computed from
 286 70 km below the continent (the same depth is employed below the oceans) to the core-
 287 mantle boundary: $d_1 = d_{\text{craton}} + 70$ where d_{craton} is given in Table 4. As the conti-
 288 nental material can deform and break apart at its edges, it could sink underneath the
 289 existing continents and give a false positive correlation in our calculations. Hence, we
 290 consider the temperature field from below a fixed distance of 70 km irrespective of con-
 291 tinental thickness. Two different depth windows are used: $w_{T1} = 2890 - d_1$ for the
 292 whole mantle and $w_{T2} = 1000 - d_1$ for the upper part of the mantle. See Fig. 1 for a
 293 schematic representation of the model setup.

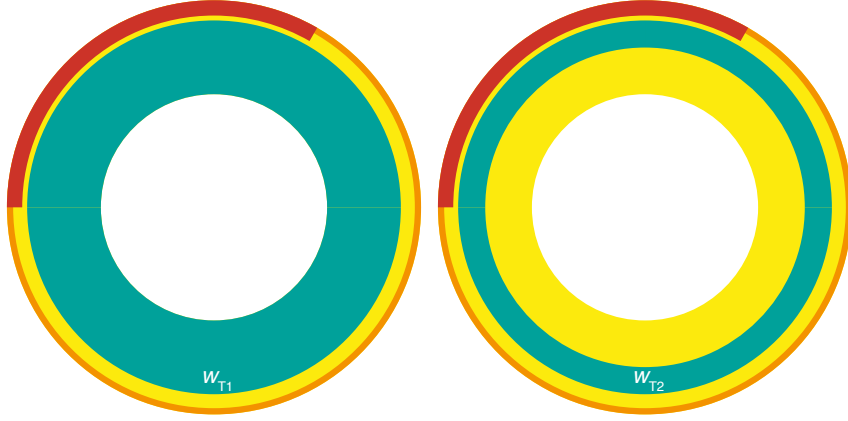
295 Using Fourier coefficients, we calculate the correlation function between the tem-
 296 perature T and composition C fields using the relation:

$$\text{corr}_{l,C,T} = \left(a_{l,C} a_{l,T} + b_{l,C} b_{l,T} \right) \frac{\pi \Delta T}{\sum_{j=1}^l 2/j}, \quad (14)$$

297 where $\Delta T = 2500$ K is a constant used to dimensionalize temperature. The factor
 298 on the right hand side of Eq. 14 is used to obtain the amplitude of the temperature anom-
 299 alies assuming discontinuous continents. This formulation helps in computing the ampli-
 300 tude of a degree l sinusoidal thermal anomaly below a Heaviside shaped continent of iden-
 301 tical degree.

305 2.6 Time-dependence of the Correlation

306 The time-dependence of the continent-temperature correlation can also be obtained
 307 using our spectral analysis. However, the result might not directly answer the question



302 **Figure 1.** Schematic representation of the model with continent (red), composition correlation
 303 window (orange), and temperature correlation windows w_T (teal) as defined in Section 2.5 (not
 304 to scale).

308 of how fast temperature can rise below a continent as the Fourier decomposition simul-
 309 taneously reports how fast the regions away from the continents cool. Yet, this spectral
 310 method gives insightful trends concerning the evolution of lateral temperature anoma-
 311 lies associated with the surface distribution of continents on a global scale.

312 Since the correlation has the dimensions of temperature, one can calculate the evo-
 313 lution of the lateral temperature anomalies for each harmonic degree. In the present study,
 314 we computed an average of the evolution of temperature anomalies over the first 6 de-
 315 grees only to avoid introducing too much noise. Thus, we used:

$$\left\langle \frac{\partial \text{corr}_{C,T}}{\partial t} \right\rangle = \frac{1}{N} \sum_{l=1}^N \frac{1}{t_{\text{max}}} \int_{t=0}^{t_{\text{max}}} \left| \frac{\partial \text{corr}_{l,C,T}}{\partial t} \right| dt \quad (15)$$

316 where N is the number of harmonics used for the average ($N = 6$ in the present study)
 317 and t_{max} is the final physical time non-renormalized by the average velocity.

318 **3 Results**

319 In order to investigate both the magnitude of temperature anomalies appearing be-
 320 low continents (together with the heating or cooling at a distance from continents) and
 321 their effects on mantle convection, we performed two sets of simulations. First, we ex-
 322 amined 33 cases considering incompressible convection with constant basal and inter-
 323 nal heating (Table 4). Second, we performed 12 simulations considering compressible con-
 324 vection with core cooling, no internal heating, melting and crustal production (Table 5).
 325 For both sets of simulations, the surface heat flow Q_{surf} and CMB heat flow Q_{cmb} re-
 326 ported in this paper are obtained by multiplying the heat fluxes obtained in 2D simu-
 327 lations by the surface area of the Earth. The heat flows can therefore be directly com-
 328 pared to Earth's values.

341 The absence of melting, and thereby the lack of consumption of latent heat in the
 342 first set of simulations allows the mantle temperatures to rise. Thus, we were able to study
 343 the effect of core temperature T_{cmb} , number of continents n_{craton} , radiogenic heating
 344 H , and reference viscosity η_0 on the amplitude of these thermal anomalies. In cases with
 345 melting and crustal production, we also observed the development of warm thermal anoma-
 346 lies below the continents, which often caused their breakup.

329 **Table 4.** Simulations featuring incompressibility with core temperature T_{cmb} (K), radiogenic
 330 heating H (W/kg), cratonic thickness d_{craton} (km), reference viscosity η_0 (Pa-s), number of
 331 continents n_{craton} , final model runtime t_r (Gyr), average velocity v_{RMS} (cm/yr), mean surface
 332 heat flow Q_{surf} (TW), mean CMB heat flow Q_{cmb} (TW), dominant degree of correlation deg ,
 333 its amplitude $corr$ (K) and the averaged evolution of the correlation $\langle \partial corr / \partial t \rangle$ (K/Gyr). For
 334 correlation, temperature field was averaged in the depth window w_{T1} for all simulations.

T_{cmb}	H	η_0	n_{craton}	d_{craton}	t_r	v_{RMS}	Q_{surf}	Q_{cmb}	deg	$corr$	$\langle \partial corr / \partial t \rangle$
2000 ^{s1,x}	0	$7.88 \cdot 10^{22}$	1	570	4.50	0.06	2.17	2.01	-	-	-
2000 ^x	0	$7.88 \cdot 10^{22}$	2	570	4.14	0.05	2.14	1.96	-	-	-
2000 ^x	0	$7.88 \cdot 10^{22}$	6	570	3.84	0.04	1.96	1.80	-	-	-
3000 ^a	0	$7.88 \cdot 10^{22}$	1	570	4.50	0.46	12.57	11.78	1	231.24	11.53
3000 ^b	0	$7.88 \cdot 10^{22}$	2	570	3.60	0.40	12.67	11.55	2	55.89	13.84
3000 ^{s2}	0	$7.88 \cdot 10^{22}$	3	570	4.50	0.39	13.74	12.08	3	3.57	37.14
3000	0	$7.88 \cdot 10^{22}$	4	570	4.50	0.35	14.10	12.66	1	17.38	21.17
3000 ^x	0	$7.88 \cdot 10^{22}$	5	570	4.50	0.33	14.14	12.86	-	-	-
3000 ^x	0	$7.88 \cdot 10^{22}$	6	570	4.50	0.26	13.72	12.91	-	-	-
4000 ^e	0	$7.88 \cdot 10^{22}$	1	570	4.50	1.81	31.67	34.61	2	10.02	43.62
4000	0	$7.88 \cdot 10^{22}$	2	570	4.50	1.50	33.26	35.34	2	9.78	45.35
4000	0	$7.88 \cdot 10^{22}$	6	570	2.69	1.29	31.06	36.19	1	7.29	37.07
2000 ^{i,x}	0	$7.88 \cdot 10^{22}$	2	570	2.23	0.05	2.62	2.22	-	-	-
3000 ^{c,i}	0	$7.88 \cdot 10^{22}$	2	570	2.93	0.36	13.22	11.63	1	65.81	15.83
4000 ^{i,x}	0	$7.88 \cdot 10^{22}$	2	570	0.89	1.03	31.57	32.88	-	-	-
3000	$3 \cdot 10^{-12}$	$7.88 \cdot 10^{22}$	1	570	4.50	1.08	20.25	12.40	1	75.71	17.47
3000	$3 \cdot 10^{-12}$	$7.88 \cdot 10^{22}$	2	570	4.50	0.78	21.25	13.09	2	20.84	20.06
3000	$3 \cdot 10^{-12}$	$7.88 \cdot 10^{22}$	6	570	4.50	0.74	21.64	13.75	1	14.47	22.02
3000 ^x	$3 \cdot 10^{-12}$	$1.57 \cdot 10^{22}$	1	335	1.60	1.57	24.79	19.39	-	-	-
3000	$3 \cdot 10^{-12}$	$1.57 \cdot 10^{22}$	2	335	4.50	1.67	28.23	20.61	2	14.98	34.23
3000	$3 \cdot 10^{-12}$	$1.57 \cdot 10^{22}$	6	335	4.50	1.77	27.75	20.97	2	3.84	41.34
3000	$3 \cdot 10^{-12}$	$7.88 \cdot 10^{21}$	1	263	4.50	2.35	29.83	23.12	1	18.34	42.12
3000	$3 \cdot 10^{-12}$	$7.88 \cdot 10^{21}$	2	263	4.50	2.24	29.16	23.38	2	6.40	44.77
3000	$3 \cdot 10^{-12}$	$7.88 \cdot 10^{21}$	6	263	4.50	2.49	29.09	24.08	1	5.67	48.08
3000 ^d	$6 \cdot 10^{-12}$	$7.88 \cdot 10^{22}$	1	570	4.50	1.88	26.52	13.20	1	54.78	27.90
3000	$6 \cdot 10^{-12}$	$7.88 \cdot 10^{22}$	2	570	4.50	1.13	29.55	14.01	2	28.24	28.43
3000	$6 \cdot 10^{-12}$	$7.88 \cdot 10^{22}$	6	570	4.50	1.29	29.49	14.71	6	-3.76	34.58
3000	$6 \cdot 10^{-12}$	$1.57 \cdot 10^{22}$	1	335	4.50	2.42	33.56	20.32	1	20.70	41.95
3000	$6 \cdot 10^{-12}$	$1.57 \cdot 10^{22}$	2	335	4.50	2.39	34.53	21.19	2	9.33	52.56
3000	$6 \cdot 10^{-12}$	$1.57 \cdot 10^{22}$	6	335	4.50	2.80	31.67	21.21	2	2.41	58.16
3000 ^{s3}	$6 \cdot 10^{-12}$	$7.88 \cdot 10^{21}$	1	263	4.50	3.05	35.74	23.70	1	17.79	59.39
3000	$6 \cdot 10^{-12}$	$7.88 \cdot 10^{21}$	2	263	4.50	2.99	36.73	24.30	2	5.64	48.99
3000	$6 \cdot 10^{-12}$	$7.88 \cdot 10^{21}$	6	263	4.50	3.44	35.82	24.83	1	6.29	52.72

^{a-e} cases presented in Section 3.1.1 and Fig. 2, 3 and 4.

^{s1-s3} additional cases presented in Appendix Fig. A.1, A.2 and A.3

^x unrealistic cases excluded from empirical regressions. See text for details.

ⁱ continents initialized 90 degrees apart.

335 **Table 5.** Simulations featuring compressibility with MCP and without internal heating. Initial
 336 core temperature T_{cmb} (K), number of continents n_{craton} , depth window for averaging tem-
 337 perature field w_{T} , average velocity v_{RMS} (cm/yr), mean surface heat flow Q_{surf} (TW), mean
 338 CMB heat flow Q_{cmb} (TW), dominant degree of correlation deg , its amplitude $corr$ (K) and the
 339 averaged evolution of the correlation $\langle \partial corr / \partial t \rangle$ (K/Gyr). Reference viscosity $\eta_0 = 1 \cdot 10^{20}$ Pa-s,
 340 cratonic thickness $d_{\text{craton}} = 231$ km, and final model runtime $t_{\text{r}} = 4.5$ Gyr for all simulations.

T_{cmb}	n_{craton}	w_{T}	v_{RMS}	Q_{surf}	Q_{cmb}	deg	$corr$	$\langle \partial corr / \partial t \rangle$
3500	1	1	1.19	16.35	5.85	1	38.86	24.22
3500 ^f	1	2	0.91	13.12	5.45	1	17.32	74.22
3500	2	1	0.89	12.63	5.68	1	56.06	27.76
3500	2	2	0.94	13.04	5.92	2	20.30	42.73
4000	1	1	2.03	18.40	12.59	1	19.62	62.78
4000 ^g	1	2	1.74	17.48	13.17	1	28.08	89.76
4000	2	1	1.52	17.77	13.31	2	13.26	59.89
4000	2	2	2.01	16.68	12.03	2	0.07	65.41
4500	1	1	1.48	18.58	13.23	7	-3.05	46.29
4500 ^h	1	2	1.50	19.02	13.33	1	23.52	85.67
4500	2	1	1.50	16.97	13.30	9	-5.47	41.89
4500	2	2	1.49	19.31	12.95	2	5.95	79.38

^g case presented in Fig. 5.

^{f-h} cases presented in Fig. 6.

347 3.1 First Set of Simulations: Incompressible Convection Without MCP

348 In this set of simulations, we systematically varied the following parameters (see
 349 Table 4):

- 350 • Constant internal heating: $H = 0, 3 \cdot 10^{-12}$ and $6 \cdot 10^{-12}$ W/kg,
- 351 • Constant core temperature: $T_{\text{cmb}} = 2000, 3000$ and 4000 K,
- 352 • Initial number of continents: 1, 2 and 6, where the sum of the continents' length
 353 is always 30% of the surface length,
- 354 • Initial position of continents: antipodal points and 90 degrees apart,
- 355 • Reference viscosity: $\eta_0 = 7.88 \cdot 10^{21}, 1.57 \cdot 10^{22}$ and $7.88 \cdot 10^{22}$ Pa-s (see Table 1
 356 for all parameters).

357 The thickness of continents is decided in accordance with the expected background
 358 lithospheric thickness as cratons on Earth have a larger thickness than the oceanic litho-
 359 sphere. Boundary layer theory (Solomatov, 1995) demonstrates that self-consistently form-
 360 ing boundary layers depend on the Rayleigh number Ra : $\delta \simeq DRa^{-1/3}$, where δ is the
 361 lithospheric thickness and D is the mantle thickness. The Rayleigh number itself depends
 362 on several quantities that are kept fixed in our simulations but also on the core to sur-
 363 face temperature difference and the internal viscosity. For simplicity, since we vary the
 364 core temperature much less than the viscosity in our parameter space, we chose to only
 365 use a viscosity-dependent continent thickness. Assuming an oceanic boundary layer thick-
 366 ness of $\delta_{\text{oceanic,E}} = 100$ km and continental boundary layer thickness of $\delta_{\text{craton,E}} =$
 367 210 km for the Earth, our oceanic and continental initial lithosphere thicknesses are ob-
 368 tained using the relation $\delta_{\text{model}} = (\eta/\eta_E)^{1/3} \cdot \delta_E$ as used previously in (Rolf & Tack-
 369 ley, 2011). This ensures that the continents are always thicker than the surrounding litho-
 370 sphere for any choice of reference viscosity. A small thermal perturbation of 125 K is in-
 371 troduced in the mid-mantle at 3 o'clock to help initiate the first upwellings. In this set

372 of simulations, a value of 1550 K is used for initial potential temperature T_{P0} , which rep-
 373 represents the temperature of a given portion of the mantle if it ascended adiabatically to
 374 the surface without undergoing melting (McKenzie & Bickle, 1988).

375 **3.1.1 Qualitative Observations**

376 Fig. 2, 3 and 4 depict the temporal evolution of five cases to help understand why
 377 and how positive temperature anomalies tend to be located below continents. Fig. 2 shows
 378 the evolution of the temperature fields and Fig. 3 represents the evolution of the corre-
 379 lation between temperature and composition field (cratons) for harmonic degrees 1 to
 380 10. Fig. 4 shows the time series of CMB heat flow Q_{cmb} , surface heat flow Q_{surf} , and
 381 the fraction of internal heating $(Q_{\text{surf}} - Q_{\text{cmb}})/Q_{\text{surf}}$. The rows of these three figures
 382 are organized as follows:

- 383 • a: 3000 K, one supercontinent, no internal heating,
- 384 • b: 3000 K, two continents initially at antipodal points, no internal heating,
- 385 • c: 3000 K, two continents initially 90 degrees apart, no internal heating,
- 386 • d: 3000 K, one supercontinent, strong internal heating ($H = 6 \cdot 10^{-12}$ W/kg).
- 387 • e: 4000 K, one supercontinent, no internal heating

388 All five cases employ a reference viscosity of $7.88 \cdot 10^{22}$ Pa.s.

389 In cases *a-e*, the initial plumes rising from the core-mantle boundary are slower be-
 390 low the continents. Away from the continents, the oceanic lithosphere is weak enough
 391 to subduct and it brings cold material down into the lower mantle. This increases the
 392 thermal contrast between the surrounding mantle and regions of plume generation and
 393 provides additional buoyancy to the plumes, which quickly diffuse their heat while reach-
 394 ing the surface. As the continents are 100 times more viscous and have 10 times the yield
 395 stress compared to the oceanic lithosphere, they do not break. The thermal contrast be-
 396 tween the subcontinental and suboceanic mantle is enhanced by the cold downwellings
 397 along continental margins and in regions away from the continents.

398 In case *a* presented in Fig. 2a, the correlation between continent and temperature
 399 field arises as soon as convection cells form due to the strength of the cratonic material
 400 and this correlation is maintained throughout the simulation with a maximum ampli-
 401 tude of 237 K.

402 Additionally, cases *b, c* with 2 continents (each covering 15% of surface area) ini-
 403 tialized at antipodal points and 90 degrees apart are also presented in Fig. 2b and 2c, re-
 404 spectively. When the 2 continents are at antipodal points, a degree-2 thermal structure
 405 is dominant in the mantle (Fig. 2b and 3b) with an episode of anti-correlation in degree-
 406 2 between 1 and 1.5 Gyr of evolution. This anti-correlation can be understood by look-
 407 ing at the third column of Fig. 2b, which shows that downwellings can be pushed to the
 408 edges of the continents and produce cold anomalies below the continents. In Fig. 2c and
 409 3c, continents are first closer to each other until 500 Myr, which generates a degree-1 cor-
 410 relation. They drift apart and form a degree-2 correlation until 1.3 Gyr and then come
 411 close again, which brings the correlation back to degree-1. These cases show that ther-
 412 mal structure of the mantle and the degree of the continent-temperature correlation fol-
 413 lows the geometrical configuration of the cratons.

414 In internally heated case *d* presented in Fig. 2d, radiogenic heating strongly increases
 415 the internal temperature with time as melting and crustal production is not employed
 416 in this simulation. For Earth, the internal temperature would be buffered by the removal
 417 of latent heat resulting from MCP. Still, one can see that downwellings preferentially stay
 418 away from continents despite the non-stationarity of the flow patterns and the efficient
 419 stirring. Correlation in degree-1 and degree-2 is observed (see also Fig. 3d).

420 In case e shown in Fig. 2e, despite the fact that a degree-1 correlation is formed,
 421 the large core temperature generates strong plumes which tend to push the continent
 422 laterally. This explains why the continent moves over a cold region (3rd column) and gen-
 423 erates an anti-correlation (see arrow in Fig. 3e).

424 As seen in the second column of each row of Fig. 2, downwellings preferentially prop-
 425 agate through the lower mantle, also below continents, but the subcontinental upper man-
 426 tle stays warm. This observation lead us to investigate the correlation using both the
 427 whole mantle and the upper part of mantle in the second set of simulations (see Fig. 1
 428 and rows 3 and 6 in Table 6). Despite the known limitations of numerical models, this
 429 observation is probably robust and applies to the Earth. Even if slabs rebound at the
 430 660 km discontinuity on Earth, they do not tend to come back up below cratons due to
 431 their weight.

442 *Effects of the Reference Viscosity and Internal Heating Rate*

443 Fig. 2d and 3d show that a degree-1 correlation below a supercontinent persists with
 444 strong internal heating but is lower in amplitude. We observe that a decrease in refer-
 445 ence viscosity (see Fig. A.1s3 and A.2s3) or an increase of internal heating rate both tend
 446 to decrease the magnitude of the correlation between continents and subcontinental man-
 447 tle temperature. In both cases, convective stirring laterally scatters thermal anomalies
 448 which intrinsically decreases the correlation. This naturally happens when the reference
 449 viscosity is low as the flow is vigorous and small wavelengths form while broader plumes
 450 are no longer present. When strong radiogenic heating is considered, strong stirring takes
 451 some time to appear as it arises from the decrease of viscosity with time.

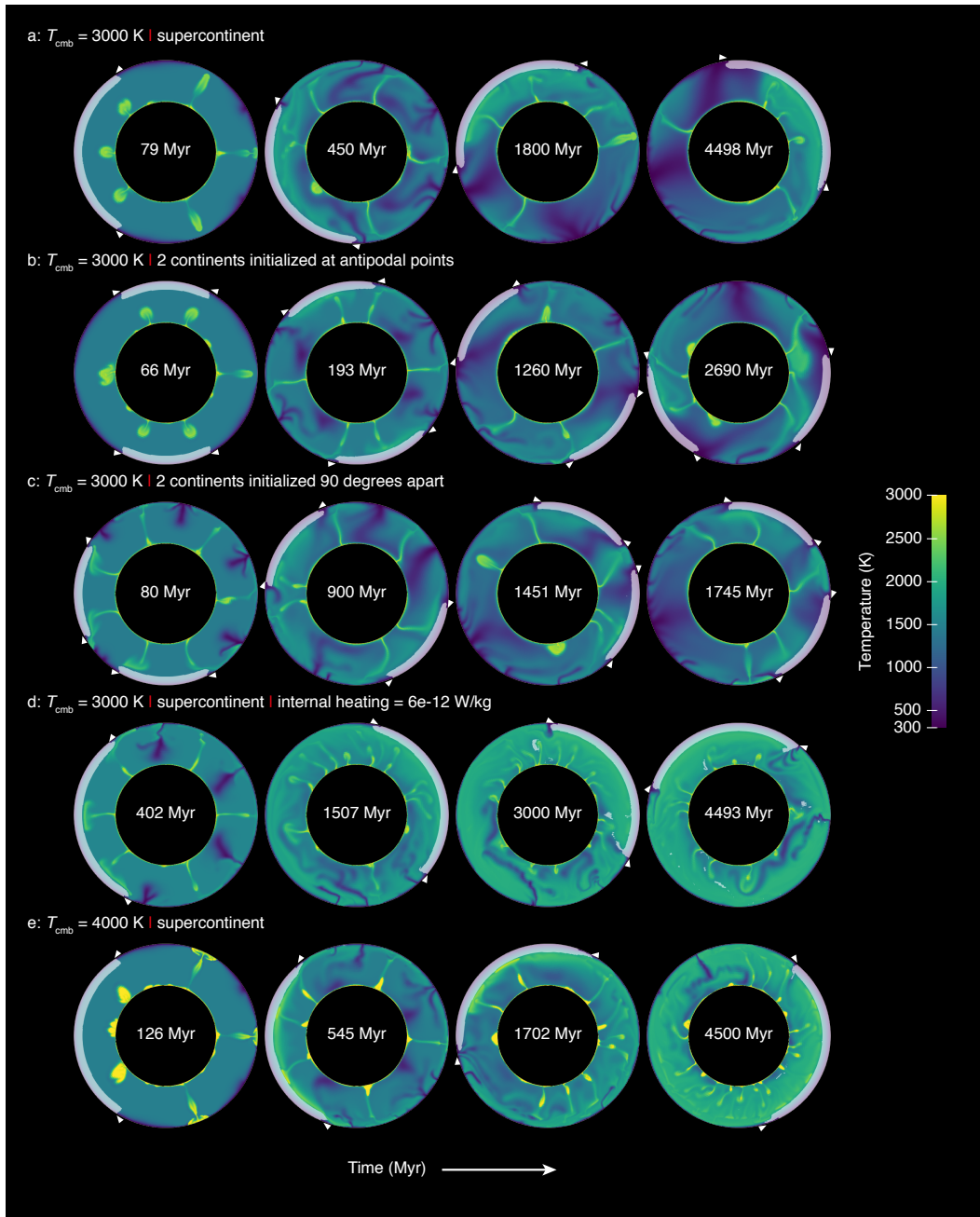
452 *Effect of the Core Temperature*

453 Cases with $T_{\text{cmb}} = 2000$ K (for example, see Fig. A.1s1 and A.2s1) show similar
 454 processes of rising mantle plumes, subduction and entrainment of cold slabs in the con-
 455 vecting mantle and a buildup of elevated temperatures in the subcontinental mantle. Yet,
 456 the low core temperature does not allow the mantle to maintain an internal tempera-
 457 ture, which is comparable to the observed present-day value. Large downwellings strongly
 458 decrease the ambient temperature well below 1000 K, which leads to an unrealistic sit-
 459 uation where the mantle has huge blobs of high viscosity and the entire lithosphere starts
 460 to drift. We do not use these cases for our empirical regressions of correlation amplitude
 461 (discussed further in Section 4.4.1). In cases with $T_{\text{cmb}} = 4000$ K (for example, see Fig. 2e
 462 and 3e), there are many more thermal instabilities at the bottom, which is expected with
 463 a hotter core. Again, the region of subcontinental mantle warming develops (seen as degree-
 464 1 correlation in Fig. 3e) but this warm thermal anomaly disappears over time due to a
 465 stronger convective flow.

470 *3.1.2 Evolution of surface and CMB heat flows*

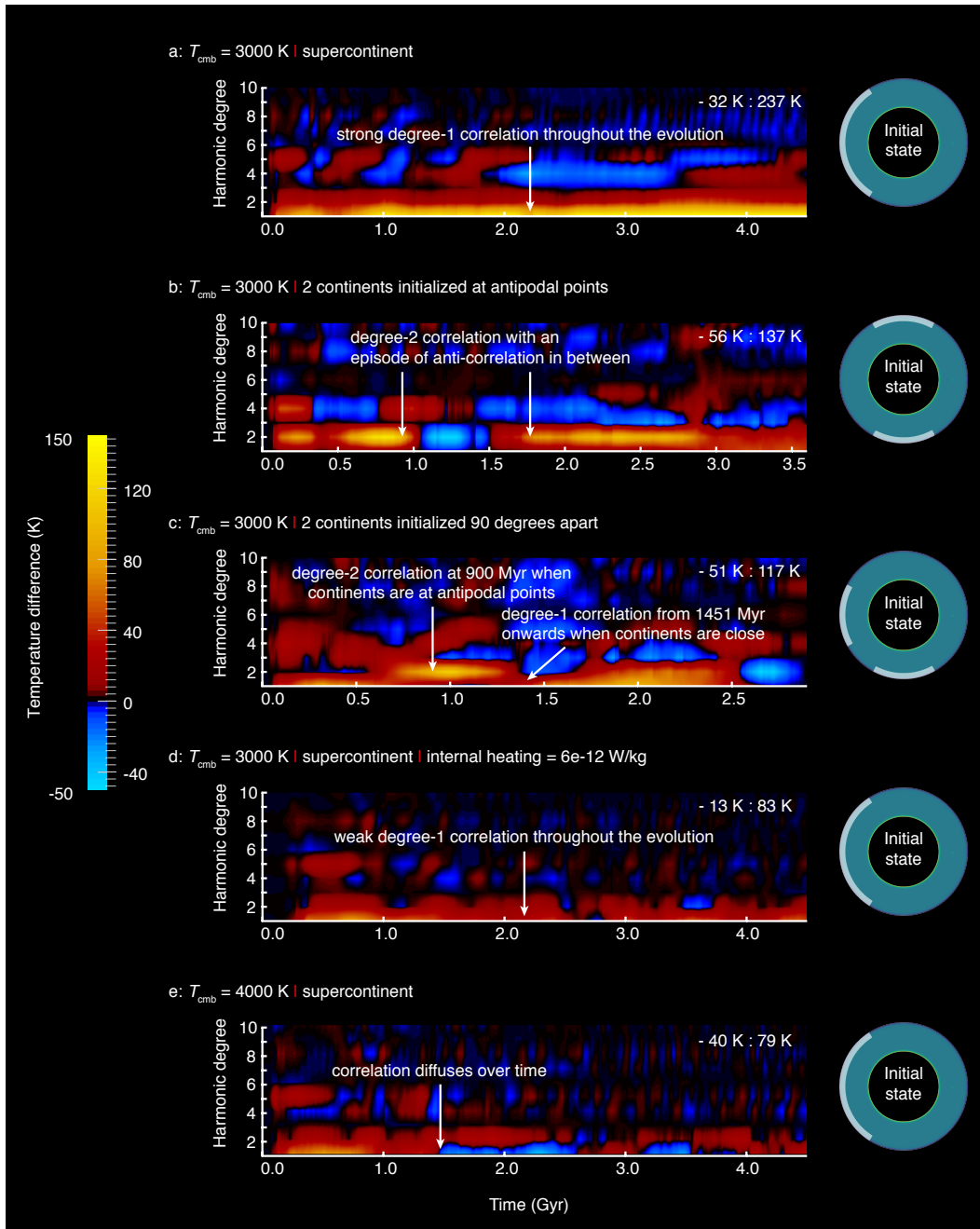
471 Fig. 4 represents the evolution of the heat flow of the simulations previously dis-
 472 cussed (Fig. 2 and 3). We display surface and CMB heat flows (see purple and green curves
 473 with left y-axis). The normalized difference between top and bottom heat flows is also
 474 shown (see yellow curve with right y-axis). This quantity reflects the evolution of aver-
 475 age temperature of the mantle in cases without internal heating and converges to zero
 476 when the equilibrium is reached. When internal heating is active, the heat flow differ-
 477 ence also reflects the amount of radiogenic heating, preventing it from reaching zero even
 478 if an equilibrium is found (as seen in Fig. 4d).

479 Fig. 4a, 4b and 4c show that the simulations excluding internal heating and con-
 480 sidering a realistic core temperature (3000 K in incompressible convection simulations
 481 correspond to ~ 4000 K in reality when considering the adiabatic temperature increase



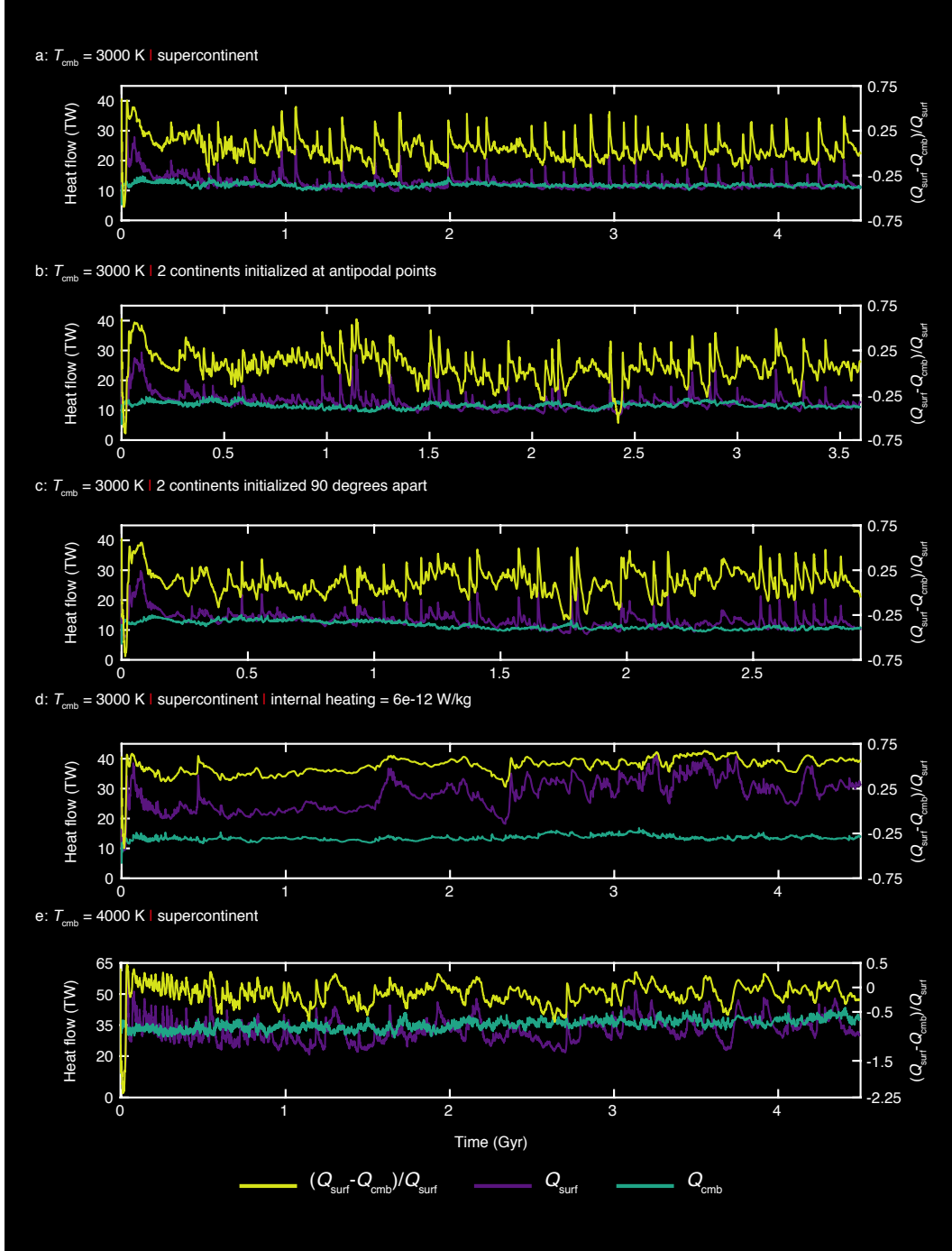
432 **Figure 2.** Thermal evolution of the cases *a-e* featuring incompressibility and without MCP.
 433 White triangles demarcate the continents, which are represented by composition field (white)
 434 superimposed over the temperature field. A small thermal anomaly of 125 K is introduced in the
 435 mid-mantle at 3 o'clock in all these models.

482 with depth) quickly reach an equilibrium. The heat flows themselves stabilize and their
 483 time-averaged difference is close to zero, with significant short-timescale fluctuations. A
 484 slight tendency for cooling is more visible in case *c* which has 2 continents initialized at
 485 non-antipodal positions. Fig. 4d shows that radiogenic heating warms up the planet. The
 486 last two billion years of evolution show the equilibrium state in which radiogenic heat-
 487 ing stabilizes the difference between surface and CMB heat flows. One can see that the



436 **Figure 3.** (left) Spectrogram of the cases *a-e* featuring incompressibility and without MCP,
 437 where positive (red to yellow) and negative (shades of blue) values indicate correlation and anti-
 438 correlation between continental material at the surface and elevated temperatures underneath
 439 respectively (using temperature correlation window w_{T1}). Also shown are the minimum and
 440 maximum temperature contrasts obtained from the models. (right) Initial state of the models
 441 with continents (white).

488 initial difference between the heat flows is lower, which means that the mantle is warm-
 489 ing up (also seen in Fig. 2d). Fig. 4e shows that the planet gradually warms up due to
 490 the large core temperature. The average heat flow difference is slightly negative and the



466 **Figure 4.** Time series of heat flow at the core-mantle boundary Q_{cmb} and at the surface
 467 Q_{surf} on the left y-axis for the cases *a-e* featuring incompressibility and without MCP. Also
 468 shown, on the right-axis is the fraction of internal heating $(Q_{\text{surf}} - Q_{\text{cmb}})/Q_{\text{surf}}$ as a function of
 469 time. Note that case e has different limits on both y-axes.

491 absolute values of heat flows slightly increase with time. This is due to the decrease in
 492 internal viscosity of the mantle. However, the heat flows do not vary more than $\sim 10\%$.

493 Although Fig. 4 depicts the general thermal evolution of the planet, we do not find
 494 a direct correlation between heat flows (or their difference) and the evolution of the continent-
 495 temperature correlation.

496 3.2 Second Set of Simulations: Compressible Convection With MCP

497 In this second set of simulations, we used a more realistic setup in which the core
 498 cools with time, and more importantly, melting and crustal production are considered.
 499 As these features result in much higher computational costs, a smaller number of sim-
 500 ulations were run in the selected parameter space.

501 The primary distinguishing aspect of these models is the inclusion of melting of py-
 502 rolytic mantle and the subsequent basaltic crustal production. Two different correlation
 503 windows w_T define the depth range over which the temperature field is averaged with
 504 $w_{T1} = 300 - 2890$ km and $w_{T2} = 300 - 1000$ km. Continental thickness is initialized
 505 as 230 km and all the cases have mixed heating with a reference viscosity $\eta_0 = 10^{20}$ Pa·s
 506 (the viscosity now also depends on pressure). The initial potential temperature is 1900 K
 507 in this set of simulations. For numerical reasons, there is no radiogenic heating in these
 508 simulations. Unlike the incompressible convection cases, no thermal anomaly is intro-
 509 duced in the models because it might lead to an artificial melting event.

510 3.2.1 Qualitative Observations

511 In this set of simulations, the mechanical behavior leading to cooling around the
 512 continents by the formation of downwellings at the continental margins is also observed
 513 but the melting and crustal production events break the continents apart and therefore
 514 destroy the correlation.

515 Fig. 5A shows the time-dependence of the correlation for harmonic degrees 1-10 while
 516 the breakup of a supercontinent is illustrated in Fig. 5B on global (annuli) and local (white
 517 boxes) scales with a further magnification of the key regions (yellow boxes) for case g
 518 (given in Table 5). A degree-1 correlation with an amplitude ~ 30 K can be seen in Fig. 5A,
 519 indicating that the subcontinental mantle is hotter than the suboceanic mantle. A spike
 520 in this correlation amplitude (up to 67 K) at time $t_1 = 713$ Myr is observed when a man-
 521 tle plume reaches the upper mantle and results in voluminous magmatism. Following this,
 522 the correlation in higher degrees albeit with lower amplitudes is observed owing to su-
 523 percontinent breakup. A quick comparison between the initial state and the later stages
 524 of the simulation shows that the continental material gets deformed and thinned over
 525 time owing to convective stresses.

526 At time $t_1 = 713$ Myr in Fig. 5B, the elevated subcontinental temperatures and the
 527 arrival of a mantle plume in the subcontinental region cause temperatures that exceed
 528 the pyrolytic mantle solidus. This results in decompression melting of the hot astheno-
 529 spheric mantle (White & McKenzie, 1989), which generates basaltic melt (light blue).
 530 If this melt is in the top 300 km, then it is instantaneously removed from this depth and
 531 placed at the surface above the continents to create oceanic crust or continental flood
 532 basalt (pink, $\geq 30\%$ in a cell) and simulate volcanic eruption (see Section 2.4 for imple-
 533 mentation details). With time, this basaltic material gets buried and transforms into eclog-
 534 ite at a depth of 60 km following the phase changes introduced in Section 2.3. Eclogite
 535 is around 190 kg/m^3 denser than olivine, and its negative buoyancy creates stresses that
 536 weaken the continents. This cold eclogitic crust along with the continental material be-
 537 comes gravitationally unstable in the lithosphere (Lourenço et al., 2016) and starts to
 538 sink into the lower mantle. As a result of this downgoing material, a return flow devel-
 539 ops in the mantle. A combination of this dense eclogitic material and the return man-
 540 tle flow thins the continent inducing a continental rift at time $t_2 = 782$ Myr. By time
 541 $t_3 = 785$ Myr, the supercontinent breaks apart into two smaller continents, which start

542 to drift in opposite directions. Following the breakup, small-scale sublithospheric con-
 543 vection (Ballmer, van Hunen, Ito, Tackley, & Bianco, 2007; Bonatti & Harrison, 1976;
 544 Buck & Parmentier, 1986; Haxby & Weissel, 1986; Marquart, Schmeling, & Braun, 1999)
 545 starts in the subcontinental mantle at time $t_4 = 793$ Myr causing further decompression
 546 melting and the continent-temperature correlation fades away. The buildup of a new cor-
 547 relation requires large-scale mantle flow reorganization, which might never happen if the
 548 continents are too small or too mobile.

549 As the thermal boundary layer grows faster in the suboceanic mantle, small-scale
 550 sublithospheric convection cells develop there earlier than time $t_1 = 713$ Myr. As a re-
 551 sult of partial melting in the suboceanic mantle, latent heat is consumed and this also
 552 contributes towards the aforementioned correlation. Supercontinent breakup happens
 553 over a period of ~ 70 Myr in the model presented here. The timing of this breakup might
 554 strongly depend on the reference viscosity, which was not tested in this set of simula-
 555 tions. In simulations with lower initial core temperature of 3500 K, similar continental
 556 breakup can last up to 300 Myr.

570 **3.2.2 Evolution of surface and CMB heat flows**

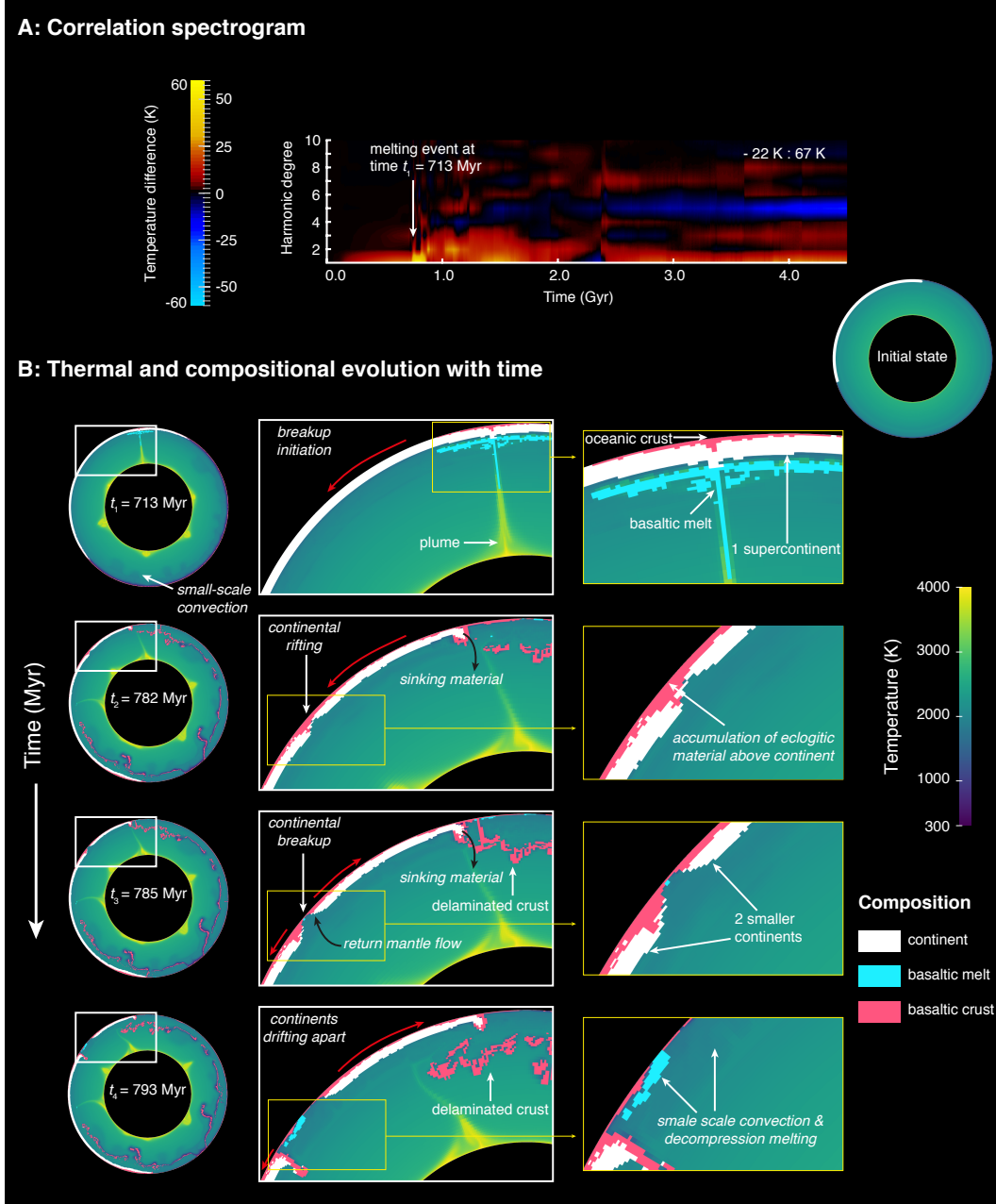
571 Fig. 6 shows the evolution of heat flow for three cases $f-h$ (given in Table 5) each
 572 with a supercontinent but with a different initial core temperature. As core cooling is
 573 considered in simulations featuring compressible convection, a decrease in the CMB heat
 574 flow Q_{cmb} is observed throughout their evolution. The positive fluctuations in the Q_{surf}
 575 are attributed to the arrival of successive mantle plumes, which cause decompression melt-
 576 ing. These fluctuations become more frequent for cases with higher initial core temper-
 577 ature as they have a larger number of thermal instabilities at the bottom boundary. The
 578 initial spikes in the Q_{surf} are because of the large amount of heat being transferred to
 579 the surface with the eruption of basaltic melt. An equilibrium regime is never reached
 580 in these simulations as the core never stops cooling. All simulations stopped with a CMB
 581 heat flow between 5 and 10 TW.

582 **4 Discussion**

583 **4.1 Empirical Regressions of the Continent-Temperature Correlation**

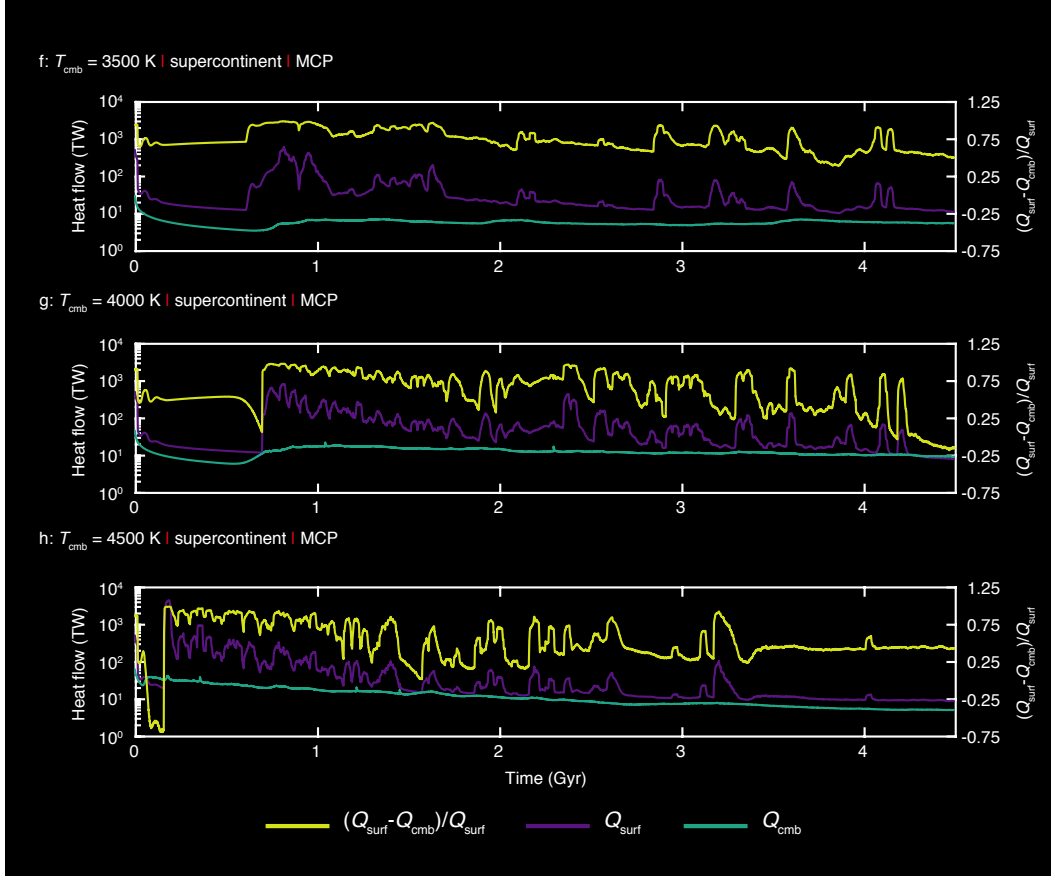
584 Our spectral decomposition of temperature and composition fields allows us to quan-
 585 tify the correlation between continents and subcontinental mantle temperature (and neg-
 586 ative temperature anomalies away from continents). Using most of the cases listed in Ta-
 587 ble 4 (see superscripts in the table for details), we were able to find a first order empir-
 588 ical equation to quantify the magnitude of the correlation. Table 6 summarizes our es-
 589 timations for the first and second sets of simulations. For the first set of simulations, 4
 590 parameters have been used to perform the regression of the correlation: T_{cmb} , n_{craton} ,
 591 H and η_0 . For the second set, H and η_0 were identical in all simulations and are there-
 592 fore absent from the regressions. Two fits are provided for the second set of simulations
 593 as we perform correlations in the entire mantle (300-2890 km) and upper part of man-
 594 tle (300-1000 km).

595 Estimating the relative impact of our input parameters on the intensity of the continent-
 596 temperature correlation is a difficult exercise as there is no physical model providing an
 597 analytical expression. Moreover, the correlation sometimes takes negative values, which
 598 makes it impossible to employ standard power law formulations as is commonly done in
 599 boundary layer theory for various quantities. We have tried various expressions to at-
 600 tempt to best fit the correlation: linear functions, power law, exponential, linear times
 601 exponential, hyperbolic tangent, etc. In all cases, many parameter combinations were
 602 tested. It appears that the regression giving the lowest standard deviation (within this
 603 small space of functions listed above) is achieved by adding a constant to the correla-
 604 tion to make it always positive and then taking the logarithm of the sum, as shown in



557 **Figure 5.** Continental breakup in a compressible convection simulation (case *g*) with MCP,
 558 4000 K CMB temperature, supercontinent, no internal heating, and correlation temperature win-
 559 dows w_{T2} . **A:** Spectrogram showing how the dominant harmonic degree changes with time. **B:**
 560 Thermal and compositional evolution with time on global (annuli) and local (white boxes) scales
 561 with a further magnification of the key regions (yellow boxes). Superimposed over the tempera-
 562 ture field are the continents (white), basaltic melt (light blue) and basaltic crust (pink, $\geq 30\%$ in
 563 a cell). Red arrows indicate the direction of continental drift. Also shown is the initial state of
 564 the simulation.

605 Table 6. This arbitrary logarithmic expression reflects the small influence of most param-
 606 eters when the correlation is low. In our tests, using a power law expression of the sum



565 **Figure 6.** Time series of heat flow at the core-mantle boundary Q_{cmb} and at the surface
 566 Q_{surf} on the left y-axis for the cases *f-h* featuring compressibility and MCP. Also shown, on the
 567 right-axis is the fraction of internal heating $(Q_{\text{surf}} - Q_{\text{cmb}})/Q_{\text{surf}}$ as a function of time. The
 568 thermal and compositional evolution along with the correlation spectrogram of case *g* is depicted
 569 in Fig. 5.

607 of the correlation with a constant gave a very similar standard deviation and showed identical
 608 relative importance of the parameters. We emphasize that the reader should not
 609 attempt to extrapolate these regressions away from the parameter window of the current
 610 study as they are not obtained from a physics-based scaling law.

611 Using our physically arbitrary formulation, we observe that an increase in T_{cmb} ,
 612 n_{craton} , and H , or a decrease in viscosity, all lead to a decrease in correlation. The dominant
 613 degree was used to fit the second set of simulations instead of the initial number
 614 of continents as the continents are split in several parts and therefore their number varies.
 615 Looking at the entire mantle, we find that the core temperature plays a negligible role
 616 in forming a correlation. Yet, the third row in Table 6 shows that the correlation between
 617 the temperature of the upper part of the mantle and the continents strongly depends on
 618 the core temperature. This shows that the plumes provide large temperature anomalies
 619 in the upper part of the mantle but contribute less to the formation of low degree patterns
 620 in the lower mantle. Moreover, broad downwellings tend to gather in the lower mantle
 621 disregarding the continental configuration at the surface due to the spherical geometry.
 622

629 **Table 6.** Empirical regressions of the continent-temperature correlation (K) and their evolu-
 630 tion (K/Gyr). $\text{corr}_{i,C,T}$ is the correlation amplitude of the degree that shows the highest value.
 631 These simple estimations are designed to show the relative importance of different parameters
 632 but are not based on a physical model. They should therefore not be physically interpreted or
 633 extrapolated.

Incompressible convection - No melting	Stand. Dev.
$\ln(\text{corr}_{i,C,T} - 6.944) = 0.732 - 2.07 \left(\frac{T_{\text{cmb}}^{-3000}}{500} \right) - 4.416 \left(\frac{n_{\text{craton}}}{3} - 1 \right)$ $- 0.893 \left(\frac{H}{2.72 \cdot 10^{-12}} - 1 \right) - 1.043 \left(\frac{1.57 \cdot 10^{22}}{\eta_0} - 1 \right)$	7.31 (K)
Compressible convection - Melting - whole mantle	Stand. Dev.
$\ln(\text{corr}_{i,C,T} - 1.148) = 0.980 - 3.154 \left(\frac{\text{degree}}{3} - 1 \right)$	6.77 (K)
Compressible convection - Melting - upper part of mantle	Stand. Dev.
$\ln(\text{corr}_{i,C,T} + 6.254) = 2.711 - 0.810 \left(\frac{\text{degree}}{3} - 1 \right) - 0.733 \left(\frac{T_{\text{cmb}}^{-4000}}{500} \right)$	4.98 (K)
Incompressible convection - No melting	Stand. Dev.
$\left\langle \frac{\text{corr}_{C,T}}{\partial t} \right\rangle = 61.97 + 22.81 \left(\log \left(\frac{1.57 \cdot 10^{22}}{\eta_0} \right) - 1 \right) + 2.56 \left(\frac{n_{\text{craton}}}{3} - 1 \right)$ $+ 13.2 \left(\frac{T_{\text{cmb}}^{-3000}}{500} \right) + 7.61 \left(\frac{H}{2.72 \cdot 10^{-12}} - 1 \right)$	7.31 (K/Gyr)
Compressible convection - Melting - whole mantle	Stand. Dev.
$\left\langle \frac{\text{corr}_{C,T}}{\partial t} \right\rangle = 61.34 + 9.05 \left(\frac{T_{\text{cmb}}^{-4000}}{500} \right) - 26.29 \left(\frac{T_{\text{cmb}}^{-4000}}{500} \right)^2$	1.83 (K/Gyr)
Compressible convection - Melting - upper part of mantle	Stand. Dev.
$\left\langle \frac{\text{corr}_{C,T}}{\partial t} \right\rangle = 87.95 + 12.03 \left(\frac{T_{\text{cmb}}^{-4000}}{500} \right) - 7.08 \left(\frac{T_{\text{cmb}}^{-4000}}{500} \right)^2$ $- 20.71 (n_{\text{craton}} - 1)$	5.30 (K/Gyr)

623 Fig. 7A plots the correlations used to perform the empirical fits (on the y-axis) ver-
 624 sus the results of the fits (x-axis). Globally, correlation amplitudes are between 0 and
 625 40 K but also reach up to 100 to 200 K. Amplitudes of correlations in simulations con-
 626 sidering melting and crustal production reach a maximum of 30 to 60 K (red squares and
 627 purple diamonds respectively). Overall, regressions are of good quality as the standard
 628 deviations are of the order of 5-7 K (see Table 6).

639 4.2 Empirical Regressions of the Evolution of the Continent-Temperature 640 Correlation

641 The last columns of Table 4 and 5 show the average evolution of the continent-temperature
 642 correlation. In Table 6 and Fig. 7B, we present empirical regressions of this evolution.

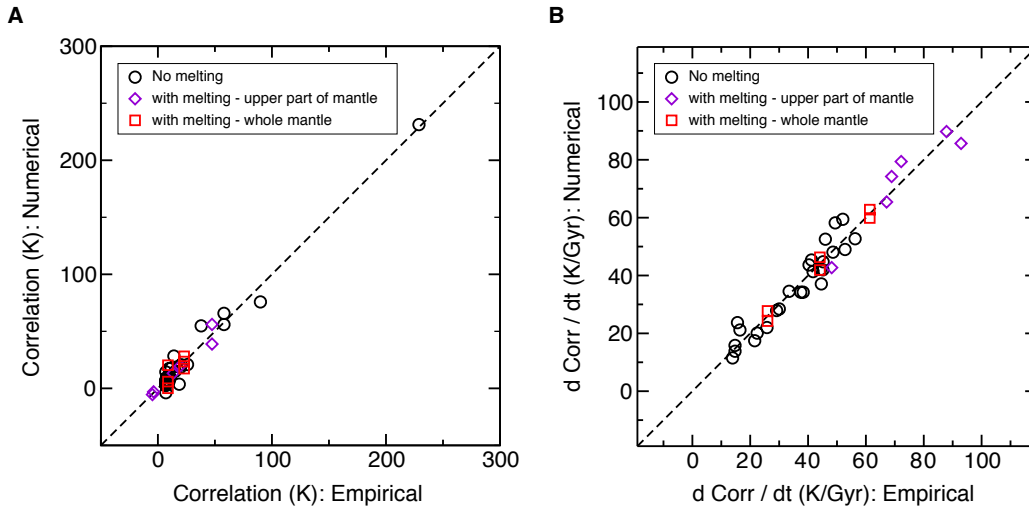
643 Concerning the spectral analysis of the evolution of continent-temperature correla-
 644 tion, two important points should be noted. First, $\langle \partial \text{corr} / \partial t \rangle$ (see Eq. 15) is not
 645 directly equal to the increase of absolute temperature below continents as it also reflects
 646 the decrease of temperature due to downwellings around the continents. Second, $\langle \partial \text{corr} / \partial t \rangle$

647 provides an average of the independent evolution of several harmonics (up to degree 6
 648 in the present study). In real space, harmonics might locally sum up and provide a much
 649 larger or much lower correlation increase. Yet, the rather low standard deviations pre-
 650 sented in Table 6 show that insightful trends and orders of magnitude can be obtained
 651 using this method.

652 Overall, it appears that the evolution of the continent-temperature correlation is
 653 on the order of 10-100 K per billion year (see Table 4, 5 and Fig. 7B). In our cases fea-
 654 turing incompressible convection, we observe that decreasing the reference viscosity or
 655 increasing the number of continents, the initial core temperature or the internal heat-
 656 ing results in an increase in the time-dependence of the correlation (see the fourth row
 657 in Table 6). Each of these contributions is discussed further.

658 A low viscosity favors both convective cooling around the cratons and their mo-
 659 bility. When the viscosity is low, downwellings can quickly cool a large volume of man-
 660 tle surrounding the regions below the cratons, resulting in a rapid growth of correlation
 661 with time. Moreover, when cratons drift above cold regions, the continent-temperature
 662 correlation also quickly drops. The kinetics of both processes are increased by lower vis-
 663 cosities.

664 Increasing the number of continents slightly increases the time-dependence of the
 665 correlation. Although this effect is minor, it might be due to the fact that numerous con-
 666 tinent are smaller in size, which makes it more difficult to maintain a potential correla-
 667 tion. A large core temperature generates warm plumes which slow down mantle cool-
 668 ing, tend to increase subcontinental mantle temperatures and push continents laterally.
 669 These three mechanisms lead to a larger time-dependence of the correlation. Finally, in-
 670 ternal heating tends to both increase the subcontinental mantle temperature and decrease
 671 the ambient viscosity. Both mechanisms lead to a high time-dependence of the correla-
 672 tion.



634 **Figure 7.** **A:** Numerical continent-temperature correlations (K) (y-axis) versus their empir-
 635 ical regressions as defined in Table 6 (x-axis) for all cases. **B:** The evolution of the correlation
 636 with time (see Eq. 15). Black circles represent the first set of simulations with no melting and
 637 crustal production, diamonds and squares depict the results of the second set of simulations.
 638 Correlations are of the order of tens to hundreds of K.

673 In compressible convection cases, looking at the entire mantle (fifth row in Table 6),
 674 we observe that the time-dependence of the correlation is maximal for a core temper-
 675 ature of 4000 K (and not 4500 K as could be expected). We chose to represent this non-
 676 linearity by a second order polynomial in our regressions (see Table 6, fifth and sixth rows).
 677 This can be explained by the fact that the lowest core temperature considered here (3500 K,
 678 for example in case *f*) does not generate very vigorous plumes. The mantle therefore cools
 679 more efficiently which increases the viscosity and slows down the kinetics of convection.
 680 On the contrary, a large core temperature (4500 K, for example in case *h*) generates such
 681 widespread magmatism that continents are rapidly destroyed. Moreover, lateral motion
 682 of the continent is observed in the simulation employing a core temperature of 4000 K
 683 (case *g*). This is due to the fact that enough crust is produced to create strong lateral
 684 density gradients in the lithosphere, leading to the mobility of the continent. When look-
 685 ing at the upper part of the mantle in compressible convection cases (sixth row in Ta-
 686 ble 6), one can see that the time-dependence of the correlation always increases with in-
 687 creasing core temperature, although we still observe some non-linearity as shown by the
 688 second order term. Overall, both the magnitude of the correlation and its time-dependence
 689 are higher when looking at the upper part of the mantle.

690 4.3 Illustration of our Regressions

691 Fig. 8 illustrates the regressions for temperature-continent correlation in the up-
 692 per part of the mantle as presented in Table 6. Since we did not systematically vary in-
 693 ternal heating and the reference viscosity in our compressible convection models, we in-
 694 ferred the influence of these parameters as determined from regressions for incompress-
 695 ible convection cases to estimate their influence on the correlation. We obtained a com-
 696 posite formulation based on both compressible and incompressible convection simula-
 697 tions which contains the four contributions of internal heating, reference viscosity, num-
 698 ber of continents and initial core temperature. We obtained the following equations:

$$\text{corr} = 6.254 + \exp \left[2.711 - 0.733 \left(\frac{T_{\text{cmb}} - 4000}{500} \right) - 0.81 \left(\frac{n_{\text{craton}}}{3} - 1 \right) - 0.893 \left(\frac{H}{2.72 \cdot 10^{-12}} \right) - 1.043 \left(\log \left(\frac{10^{21}}{\eta_0} \right) - 1 \right) \right] \quad (16)$$

$$\left\langle \frac{\text{corr}_{\text{C,T}}}{\partial t} \right\rangle = 87.95 + 12.03 \left(\frac{T_{\text{cmb}} - 4000}{500} \right) - 7.08 \left(\frac{T_{\text{cmb}} - 4000}{500} \right)^2 - 20.71 (n_{\text{craton}} - 1) + 22.81 \left(\ln \left(\frac{10^{21}}{\eta_0} \right) - 1 \right) + 7.61 \left(\frac{H}{2.72 \cdot 10^{-12}} \right) \quad (17)$$

699 Fig. 8 represents the correlations obtained using our regression (Eq. 16). The im-
 700 pact of initial core temperature on the correlation is represented for an Earth-like range.
 701 Initial core temperature in the Archean Earth was most probably higher than the present-
 702 day value which is considered to be close to 4000 K. We show how the correlation decreases
 703 with core temperature. Fig. 8 also shows that increasing the viscosity by a factor 2 adds
 704 5-15 K to the temperature anomalies below continents. Suppressing internal heating in-
 705 creases the correlation by 10-30 K. Considering 2 cratons instead of 1 supercontinent only
 706 decreases the temperature anomalies by few K. Again one should keep in mind that these
 707 absolute values are an average of the low degrees which are potentially locally additive.

708 Eq. 17 shows that a large core temperature tends to make the correlation very time-
 709 dependent. On the contrary, a low core temperature generates larger correlations sub-
 710 ject to slower evolutions. Increasing the viscosity by a factor 2 or removing internal heat-
 711 ing slows down the oscillations by a factor 2 for the reference case represented in Fig. 8.

712 Finally, considering 2 cratons instead of 1 tends to slightly slow down the evolution al-
 713 though it decreases the correlation itself.



714 **Figure 8.** Illustration of the empirical regressions: Continent-temperature correlations as a
 715 function of initial core temperature. The set of parameters representing the reference case is:
 716 $\eta_0 = 10^{20}$ Pa.s, $H = 3 \cdot 10^{-12}$ W/kg, 1 craton and $T_{\text{cmb}} = 4000$ K.

717 4.4 Implications of our Results

718 Even though our global models are rather simplified when compared to the real Earth,
 719 they help us understand and make general remarks on the long-term thermal and me-
 720 chanical influence of continents on the underlying mantle and vice versa. In this section,
 721 we illustrate the significance of our results and support them by comparing them to ge-
 722 ological and geophysical observations as well as previous numerical studies.

723 4.4.1 Previous Work, Model Parameters and Seismic Observations

724 Our models show that continents are capable of trapping heat in the underlying
 725 mantle causing subcontinental mantle warming. The amplitude of this warming changes
 726 with continental extent, CMB temperature, reference viscosity and internal heating. A
 727 higher amplitude is observed with a supercontinent (up to 237 K, see Fig 3a) and it de-
 728 creases with smaller extent of the continents. This finding agrees with the previous re-
 729 sults of Coltice et al. (2007); Lenardic et al. (2011); O’Neill et al. (2009); B. R. Phillips
 730 and Coltice (2010); Rolf et al. (2012) all of whom reported elevated temperatures be-
 731 low continents in their numerical studies. Furthermore, our models show that such ther-
 732 mal anomalies in the subcontinental mantle can persist for hundreds of millions of years
 733 and even when the continents are mobile. In all our models, the development of subduc-
 734 tion zones along continental margins helps in enhancing the thermal contrast between
 735 subcontinental and suboceanic mantle. Similar behavior has been observed in the prior
 736 work of Heron and Lowman (2011); Heron, Lowman, and Stein (2015); Lenardic et al.
 737 (2011); O’Neill et al. (2009).

738 We have tested the impact of basal heating on correlation by initializing our mod-
 739 els with different CMB temperature at the bottom boundary. The need to test this arises
 740 due to the uncertain nature and contribution of CMB heat flow towards mantle dynam-
 741 ics. Continental motion is attributed to the viscous stresses imparted by the convect-

ing mantle and the extent of this motion depends on the heat budget of the mantle. CMB heat flow, internal heating from decay of radioactive elements in the mantle, and secular mantle cooling contribute to this heat budget. Recent indications that the core's thermal conductivity may be three times higher than previously inferred mineral physics estimates (de Koker, Steinle-Neumann, & Vlcek, 2012; Gomi et al., 2013; Pozzo, Davies, Gubbins, & Alfe, 2013) and the inclusion of the post-perovskite phase change in the lower mantle (Hernlund, Thomas, & Tackley, 2005) constrain the heat flow from the core to be in the range of 10-16 TW (Hernlund, 2010; Lay, Hernlund, & Buffett, 2008; Lay, Hernlund, Garnero, & Thorne, 2006; van der Hilst et al., 2007) (although a lower core thermal conductivity has been advocated by Zhang, Cohen, and Haule (2015)). Some mantle convection models (Leng & Zhong, 2008; Mittelstaedt & Tackley, 2006; S. J. Zhong, 2006) have shown that plume heat flux can account for a significant fraction of the CMB heat flux and plume heat flux decreases by as much as a factor of 3 as the plumes ascend to the upper mantle, implying that mantle plumes should be considered when studying mantle dynamics coupled with continents.

Table 4 gives the CMB heat flow and v_{RMS} of the whole mantle for all the cases featuring incompressible convection averaged over their simulation time. Cases with $T_{\text{cmb}} = 3000 \text{ K}$ give CMB heat flow and v_{RMS} of the order of 11-13 TW and 0.25-0.45 cm/yr respectively. The heat flow values obtained from these models are in agreement with the recent heat flow estimates as discussed above and the low root-mean-square velocity of the whole mantle can be attributed to the lack of internal heating. Our models without internal heating show a general trend of decreasing correlation with increasing T_{cmb} . Comparing the CMB heat flow from these models with the recent heat flow estimates, we argue that CMB temperatures of 2000 K or 4000 K are not realistic values in an incompressible convection setup. Moreover, it should be noted that in an incompressible convection model with $T_{\text{surf}} = 300 \text{ K}$ and $T_{\text{cmb}} = 3000 \text{ K}$, the entire 2700 K superadiabatic temperature difference will drive convection whereas in a compressible convection model, around 1000-1200 K of the difference between the CMB and surface temperatures will be taken up by an adiabatic temperature increase and only the remaining 1500-1700 K will drive convection. This implies that a given T_{cmb} in an incompressible convection model will give similar behavior (e.g. in terms of plumes excess temperature) to one about 1000-1200 K higher in a compressible convection model.

When included, internal heating increases the effective convective vigor of the mantle and makes for a drastic change in the style of mantle dynamics. The internal temperature is higher and a decrease in the number of slabs stagnating at the lower boundary is observed. The more effective mantle mixing lowers the thermal isolation between the subcontinental and the suboceanic mantle. Compared to the models with only basal heating, the amplitude of degree-1 decreases (Fig. 3d and A.2s3) and for cases with low reference viscosity, no correlation is observed. This is in agreement with the main findings of Heron and Lowman (2014) who also report a decreasing influence of continental insulation on subcontinental warming with increasing Ra .

Numerous seismic tomographic studies (e.g., Grand, 2002; Houser, Masters, Shearer, & Laske, 2008; Li & Romanowicz, 1996; Masters, Laske, Bolton, & Dziewonski, 2000; Panning & Romanowicz, 2006; Ritsema, Deuss, van Heijst, & Woodhouse, 2011; Ritsema, van Heijst, & Woodhouse, 1999; Su & Dziewonski, 1997; Su, Woodward, & Dziewonski, 1994; van der Hilst, Widiyantoro, & Engdahl, 1997; Zhao, 2004) have unanimously observed slow S-wave velocity anomalies beneath present-day Africa and South Pacific, indicating a degree-2 structure for the Earth's mantle. Though our models only show a dominant degree-1 structure with a supercontinent (Fig. 2a and 3a) and degree-2 with 2 continents (Fig. 2b and 3b), these qualitative observations from our models might have been relevant in early geological history.

793 4.4.2 Continental Rifting and Flood Basalts

794 It has been suggested that mantle plumes can cause intense magmatic activity while
 795 emplacing continental flood basalts (CFB) followed by continental rifting and fragmen-
 796 tation (Campbell & Griffiths, 1990; Condie, 2004; Morgan, 1972; Richards et al., 1989;
 797 Scrutton, 1973; White & McKenzie, 1989). Studies have also shown the propensity of
 798 plumes to rise and concentrate under the relatively hotter subcontinental mantle (e.g.,
 799 Guillou & Jaupart, 1995; Gurnis, 1988; Lowman & Jarvis, 1993, 1996; B. Phillips & Bunge,
 800 2005; S. Zhong & Gurnis, 1993).

801 Flood basalts are large accumulation of basaltic lava formed in a series of large erup-
 802 tions lasting for about 1-10 Myr (V. E. Courtillot & Renne, 2003) and covering stretches
 803 of continents or oceanic floor. Prominent examples of CFB include the 65 Ma Deccan
 804 Traps in India that coincide with the opening of the NW Indian Ocean (V. Courtillot
 805 et al., 1986, 1988), the 200 Ma Central Atlantic Margin Province (CAMP) flood basalts
 806 that coincide with the opening of the Central Atlantic Ocean (V. Courtillot, Jaupart,
 807 Manighetti, Tapponnier, & Besse, 1999) and the 250 Ma Siberian Traps (Wooden et al.,
 808 1993). Examples of flood basalts that were emplaced without continental rifting are the
 809 Ontong Java Plateau (Neal, Mahoney, Kroenke, Duncan, & Petterson, 1997) and Columbia
 810 River basalts (Hooper, Camp, Reidel, & Ross, 2007; Rampino & Stothers, 1988).

811 Anderson (1982) proposed that continental assembly would cause subcontinental
 812 mantle warming and the breakup of Pangea, thereby offering an alternative source of CFB.
 813 The purely internally-heated models of Coltice et al. (2009, 2007) supported and quan-
 814 tified this proposal without the involvement of mantle plumes. They showed continental-
 815 aggregation induced elevated subcontinental mantle temperatures and large-scale melt-
 816 ing events might have caused the emplacement of CAMP flood basalts following Pangea's
 817 breakup.

818 Our model featuring compressibility with melting and crustal production presented
 819 in Fig. 5b favors the mantle plume origin for the origin of continental flood basalts. The
 820 plumes that rise up to the upper mantle result in voluminous magmatism, producing a
 821 basaltic crust. This basaltic material transforms into denser eclogite at a depth of 60 km
 822 and starts to sink into the mantle, generating a return mantle flow. The eclogitic crust
 823 combined with the return mantle flow induce continental rifting and breakup. This sce-
 824 nario represents a mix of both passive (lithospheric extension by plate forces) and ac-
 825 tive (mantle plume) rifting volcanism as proposed by Sengör and Burke (1978). These
 826 results are in contrast to the findings of O'Neill et al. (2009) who did not observe any
 827 voluminous volcanism and supercontinent breakup in their simulations. These volumi-
 828 nous basalt generating events in our model can be likened to the emplacement of CAMP
 829 continental flood basalts following the breakup of Pangea. To summarize, MCP plays
 830 a vital role in the evolution of continent-temperature correlation in two different ways.
 831 It increases the correlation by consuming latent heat and effectively cooling the subo-
 832 ceanic mantle. It decreases the correlation as decompression melting underneath the con-
 833 tinentals result in voluminous magmatism, which is followed by continental rifting and breakup.
 834 Moreover, the development of small-scale sublithospheric convection cells reduces the ther-
 835 mal contrast between the subcontinental and suboceanic mantle, which is in alignment
 836 with the findings of O'Neill et al. (2009).

837 Geological evidence also points towards the eruption of ultramafic mantle-derived
 838 volcanic rocks such as komatiites (Nisbet, 1982) above Archean greenstone belts (pri-
 839 mordial continents), for example in the Yilgarn craton of Western Australia (Mole et al.,
 840 2014; Wang, Schi tte, & Campbell, 1996) and the Dharwar craton of Southern India (Jayananda,
 841 Kano, Peucat, & Channabasappa, 2008). Our models with MCP can also be applied to
 842 such scenarios.

843 In the past, many studies of models featuring varying complexity have tried to an-
 844 swer the question of whether continents warm up the subcontinental mantle. We con-
 845 tribute to this discussion by offering qualitative observations from 2D mantle convection
 846 simulations with mobile continents. Furthermore, we provide numbers quantifying the
 847 magnitude of this continent-temperature correlation and its time-dependence by employ-
 848 ing simple empirical regressions. Starting with simple incompressible convection mod-
 849 els, we show that the dominant degree of correlation changes with continental distribu-
 850 tion and subcontinental temperature amplitude can reach up to 200 K, depending on the
 851 extent of the continents. It should be noted that this result was obtained over long time
 852 scales and with a convective vigor much less compared to the real Earth. We also show
 853 that this correlation decreases with increasing core temperature, number of continents,
 854 radiogenic heat production, or decreasing reference viscosity. These results reaffirm the
 855 previous findings of Heron and Lowman (2014); Lenardic et al. (2011); O’Neill et al. (2009);
 856 B. R. Phillips and Coltice (2010); Rolf et al. (2012). When using a more realistic setup
 857 with compressible convection, core cooling and MCP, our models demonstrate the im-
 858 pact of magmatism on the dynamics of continents. We observe that decompression melt-
 859 ing in the mantle as a result of a mantle plume or small-scale sublithospheric convection
 860 leads to voluminous volcanism. The emplacement of dense-eclogite material at the sur-
 861 face breaks the continents apart and drastically reduces this correlation (amplitude of
 862 tens of K).

863 These models have, however, some limitations, which should be addressed in fu-
 864 ture studies. Continents do not break in our incompressible convection models because
 865 they have a higher yield stress and higher viscosity than non-continental material. Ac-
 866 cordingly, the reader should not make inferences about the timings and the related ef-
 867 fects of supercontinent assembly or breakup from these models. When supercontinents
 868 do rift owing to magmatism in compressible convection simulations with MCP, the du-
 869 ration of this rifting depends on the initial core temperature. If these models were mi-
 870 grated to three dimensions, then the expected diminished effects of plumes in the up-
 871 per mantle and subducting slabs in the lower mantle would likely result in more homoge-
 872 nous mantle temperature profiles and lower correlation amplitudes. Further modeling
 873 efforts should also include real continental growth by differentiation of the mantle, in-
 874 stead of using prescribed continents. In this study, we considered fully eruptive magma-
 875 tism. In the future, the influence of plutonism on this correlation should be explored as
 876 it has been shown to play an important role in shaping the Earth’s lithosphere (Ca-
 877 wood, Hawkesworth, & Dhuime, 2013; Crisp, 1984; Rozel, Golabek, Jain, Tackley, & Gerya,
 878 2017).

879 5 Conclusions

880 We present new tools to quantify the time-dependent correlation between conti-
 881 nents and the underlying mantle, then use them to advance our understanding of the mag-
 882 nitude and causes of this correlation and its time-dependence, compared to the more qual-
 883 itative findings of previous modeling studies.

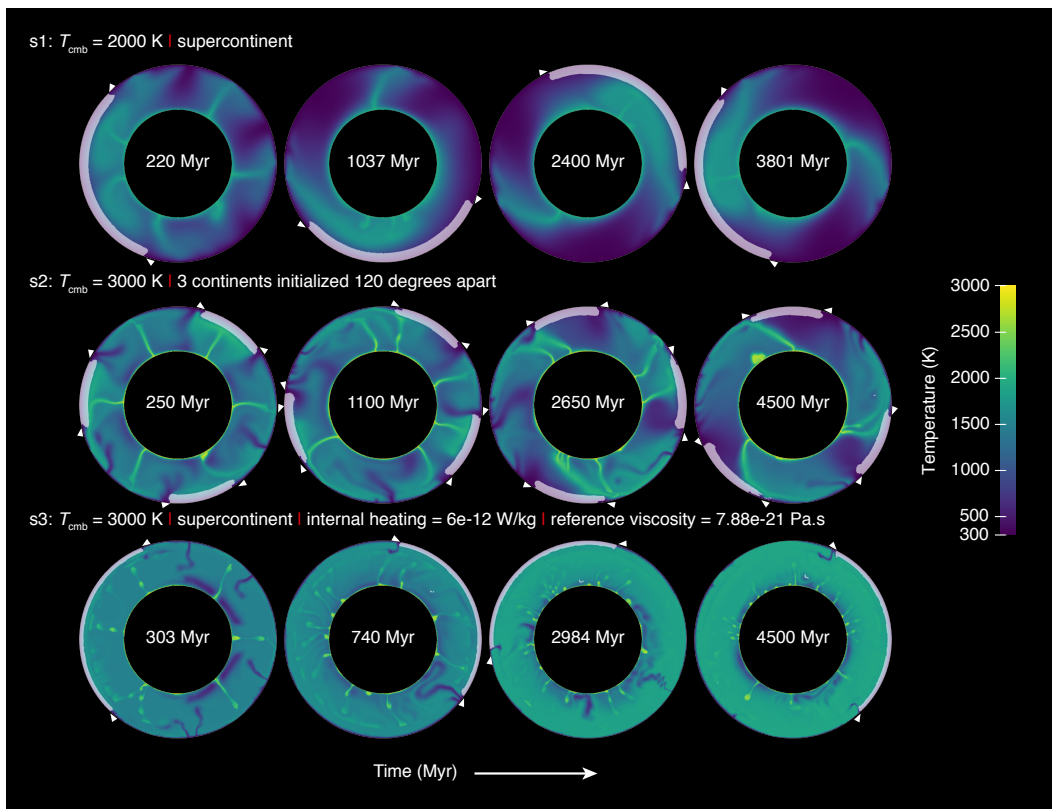
884 We first apply them to incompressible models with a complexity very similar to that
 885 considered in the large body of published literature on the influence of continents on man-
 886 tle convection. We demonstrate that the correlation between continents and the under-
 887 lying mantle is systematic, predictable and quantifiable using the tools presented in this
 888 study. Furthermore we show that an analytical fit to both the time-averaged value and
 889 the time rate of change of this correlation is possible, and give the mathematical form
 890 and best-fitting coefficients. The correlation between continents and the underlying man-
 891 tle is almost always positive, with a magnitude that decreases with increasing core tem-
 892 perature, number of continents, radiogenic heat production, and decreasing reference vis-
 893 cosity. The time rate of change of the correlation increases with increasing number of

894 continents, initial core temperature or internal heating rate, or decreasing reference vis-
 895 cosity.

896 With the aid of heat flow time-series, we show that the incompressible convection
 897 models rapidly reach statistically steady-state and therefore the long-term statistical be-
 898 havior is not influenced by the initial conditions.

899 We then apply the tools to a model setup more realistic than previously used in
 900 any studies of mantle convection with continents, one that incorporates compressibility,
 901 melting-induced crustal production, and core cooling. The above conclusions about cor-
 902 relations still apply to these models but they produce correlations that are much smaller
 903 in amplitude than the simpler, incompressible setup, a finding that points the way to-
 904 wards needed future research. These compressible convection models also exhibit con-
 905 tinental rifting and breakup, thereby supporting the mantle plume origin of continen-
 906 tal flood basalts.

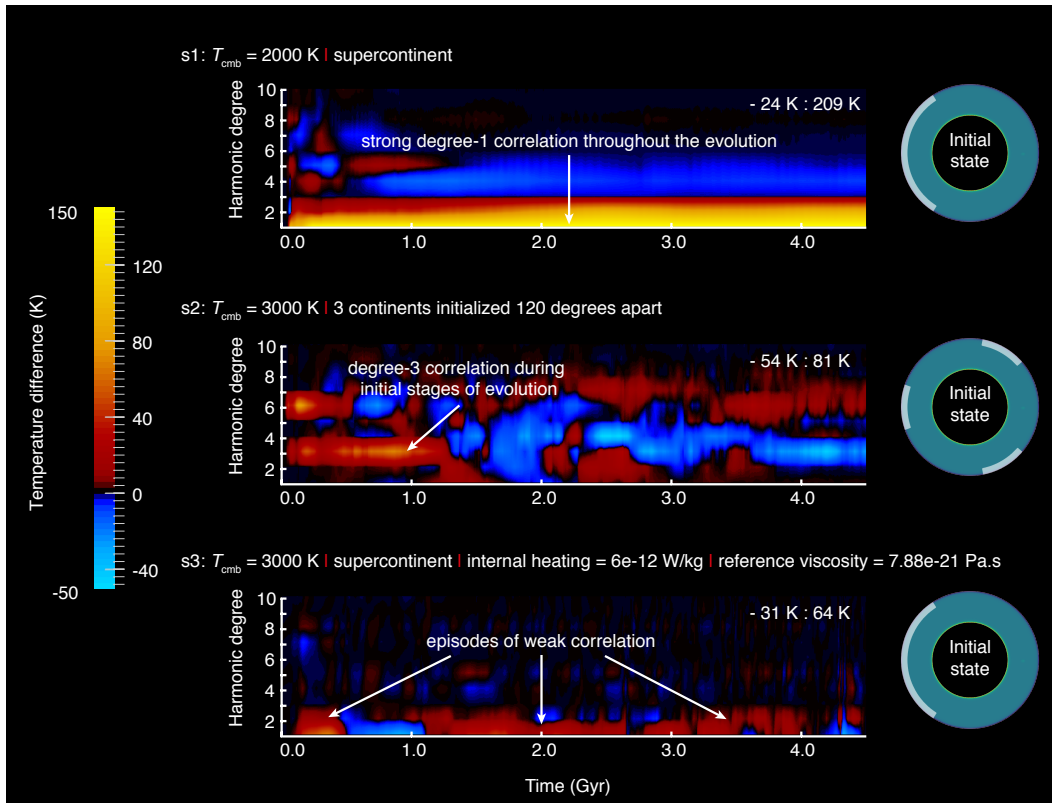
907 A Additional figures



908 **Figure A.1.** Thermal evolution of the additional cases *s1-s3* featuring incompressibility and
 909 without MCP. White triangles demarcate the continents, which are represented by composi-
 910 tion field (white) superimposed over the temperature field. A small thermal anomaly of 125 K is
 911 introduced in the mid-mantle at 3 o'clock in all these models.

922 Acknowledgments

923 We thank Adrian Lenardic, Allen McNamara, and two anonymous reviewers for their
 924 constructive reviews that helped improve the manuscript, and Thorsten Becker for his

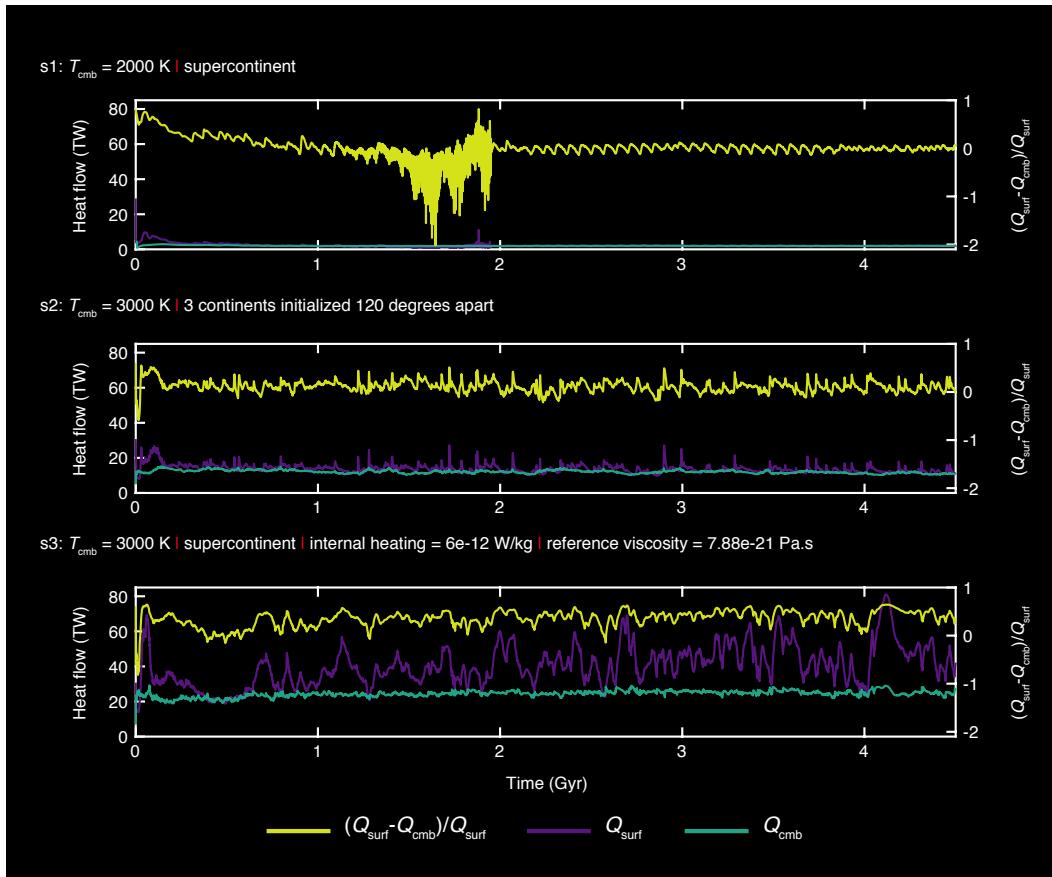


912 **Figure A.2.** (left) Spectrogram of the additional cases *s1-s3* featuring incompressibility and
 913 and without MCP, where positive (red to yellow) and negative (shades of blue) values indicate corre-
 914 lation and anti-correlation between continental material at the surface and elevated temperatures
 915 underneath respectively (using temperature correlation window w_{T1}). Also shown are the mini-
 916 mum and maximum temperature contrasts obtained from the models. (right) Initial state of the
 917 models with continents (white).

925 editorial work. C. Jain and A.B. Rozel received funding from the European Research Coun-
 926 cil under the European Union's Seventh Framework Programme (FP/2007-2013)/ERC
 927 Grant Agreement number 320639 project iGEO. The raw data from the calculations, which
 928 are visualized and analyzed in this manuscript appear in the tables found in the support-
 929 ing information. Further detail is available by contacting the corresponding author.

930 References

- 931 Amestoy, P. R., Duff, I. S., & L'Excellent, J. Y. (2000). Multifrontal parallel dis-
 932 tributed symmetric and unsymmetric solvers. *Computer Methods in Applied*
 933 *Mechanics and Engineering*, *184*(2-4), 501–520.
- 934 Ammann, M. W., Brodholt, J. P., Wookey, J., & Dobson, D. P. (2010, May). First-
 935 principles constraints on diffusion in lower-mantle minerals and a weak D''
 936 layer. *Nature*, *465*(7297), 462–465.
- 937 Anderson, D. L. (1982). Hotspots, Polar Wander, Mesozoic Convection and the
 938 Geoid. *Nature*, *297*(5865), 391–393.
- 939 Ballmer, M. D., van Hunen, J., Ito, G., Tackley, P. J., & Bianco, T. A. (2007,
 940 December). Non-hotspot volcano chains originating from small-scale sublitho-
 941 spheric convection. *Geophysical Research Letters*, *34*(23), n/a–n/a.



918 **Figure A.3.** Time series of heat flow at the core-mantle boundary Q_{cmb} and at the surface
 919 Q_{surf} on the left y-axis for the additional cases *s1-s3* featuring incompressibility and without
 920 MCP. Also shown, on the right-axis is the fraction of internal heating $(Q_{\text{surf}} - Q_{\text{cmb}})/Q_{\text{surf}}$ as a
 921 function of time.

- 942 Bonatti, E., & Harrison, C. G. A. (1976, September). Hot lines in the Earth's man-
 943 tle. *Nature*, *263*(5576), 402–404.
- 944 Boyd, F. R. (1987). High-and low-temperature garnet peridotite xenoliths and their
 945 possible relation to the lithosphere-asthenosphere boundary beneath Africa. In
 946 P. H. Nixon (Ed.), *Mantle xenolith* (pp. 403–412). John Wiley & Sons Ltd.
- 947 Boyd, F. R. (1989, December). Compositional distinction between oceanic and cra-
 948 tonic lithosphere. *Earth and Planetary Science Letters*, *96*(1-2), 15–26.
- 949 Buck, W. R., & Parmentier, E. M. (1986). Convection beneath young oceanic litho-
 950 sphere: Implications for thermal structure and gravity. *Journal of Geophysical*
 951 *Research*, *91*(B2), 1961–1974.
- 952 Buffett, B. A., Huppert, H. E., Lister, J. R., & Woods, A. W. (1992). Analytical
 953 Model for Solidification of the Earth's Core. *Nature*, *356*(6367), 329–331.
- 954 Buffett, B. A., Huppert, H. E., Lister, J. R., & Woods, A. W. (1996, April). On
 955 the thermal evolution of the Earth's core. *Journal of Geophysical Research*,
 956 *101*(B4), 7989–8006.
- 957 Campbell, I. H., & Griffiths, R. W. (1990, July). Implications of mantle plume
 958 structure for the evolution of flood basalts. *Earth and Planetary Science Let-*
 959 *ters*, *99*(1-2), 79–93.
- 960 Cawood, P. A., Hawkesworth, C. J., & Dhuime, B. (2013). The continental record

- 961 and the generation of continental crust. *Geological Society of America Bulletin*,
 962 125(1-2), 14–32.
- 963 Chandrasekhar, S. (1961). *Hydrodynamic and Hydromagnetic Stability*. New York:
 964 Oxford University Press.
- 965 Christensen, U. R., & Hofmann, A. W. (1994). Segregation of subducted oceanic
 966 crust in the convecting mantle. *Journal of Geophysical Research: Solid Earth*
 967 (1978–2012), 99(B10), 19867–19884.
- 968 Čížková, H., van den Berg, A. P., Spakman, W., & Matyska, C. (2012, June). The
 969 viscosity of Earth’s lower mantle inferred from sinking speed of subducted
 970 lithosphere. *Physics of the Earth and Planetary Interiors*, 200–201, 56–62.
- 971 Coltice, N., Bertrand, H., Rey, P., Jourdan, F., Phillips, B. R., & Ricard, Y. (2009,
 972 June). Global warming of the mantle beneath continents back to the Ar-
 973 chaeon. *Gondwana Research*, 15(3-4), 254–266.
- 974 Coltice, N., Phillips, B. R., Bertrand, H., Ricard, Y., & Rey, P. (2007). Global
 975 warming of the mantle at the origin of flood basalts over supercontinents. *Ge-*
 976 *ology*, 35(5), 391.
- 977 Coltice, N., Rolf, T., Tackley, P. J., & Labrosse, S. (2012, April). Dynamic Causes
 978 of the Relation Between Area and Age of the Ocean Floor. *Science*, 336(6079),
 979 335–338.
- 980 Condie, K. C. (2004). Supercontinents and superplume events: distinguishing signals
 981 in the geologic record. *Physics of the Earth and Planetary Interiors*, 146(1-2),
 982 319–332.
- 983 Cooper, C. M., Lenardic, A., & Moresi, L. (2006). Effects of continental insulation
 984 and the partitioning of heat producing elements on the Earth’s heat loss. *Geo-*
 985 *physical Research Letters*, 33(13), 4741.
- 986 Cooper, C. M., Moresi, L. N., & Lenardic, A. (2013, June). Effects of continental
 987 configuration on mantle heat loss. *Geophysical Research Letters*, 40(11), 2647–
 988 2651.
- 989 Courtillot, V., Besse, J., Vandamme, D., Montigny, R., Jaeger, J.-J., & Cappetta, H.
 990 (1986, November). Deccan flood basalts at the Cretaceous/Tertiary boundary?
 991 *Earth and Planetary Science Letters*, 80(3-4), 361–374.
- 992 Courtillot, V., Féraud, G., Maluski, H., Vandamme, D., Moreau, M. G., & Besse,
 993 J. (1988, June). Deccan flood basalts and the Cretaceous/Tertiary boundary.
 994 *Nature*, 333(6176), 843–846.
- 995 Courtillot, V., Jaupart, C., Manighetti, I., Tapponnier, P., & Besse, J. (1999,
 996 March). On causal links between flood basalts and continental breakup. *Earth*
 997 *and Planetary Science Letters*, 166(3-4), 177–195.
- 998 Courtillot, V. E., & Renne, P. R. (2003, January). On the ages of flood basalt
 999 events. *Comptes Rendus Geoscience*, 335(1), 113–140.
- 1000 Crisp, J. A. (1984). Rates of Magma Emplacement and Volcanic Output. *Journal of*
 1001 *Volcanology and Geothermal Research*, 20(3-4), 177–211.
- 1002 Davies, G. (2007). Thermal Evolution of the Mantle. In *Volume 9: Evolution of the*
 1003 *earth* (pp. 197–216). Elsevier.
- 1004 de Koker, N., Steinle-Neumann, G., & Vlcek, V. (2012, March). Electrical resistivity
 1005 and thermal conductivity of liquid Fe alloys at high P and T, and heat flux
 1006 in Earth’s core. *Proceedings of the National Academy of Sciences*, 109(11),
 1007 4070–4073.
- 1008 Gomi, H., Ohta, K., Hirose, K., Labrosse, S., Caracas, R., Verstraete, M. J., & Hern-
 1009 lund, J. W. (2013, November). The high conductivity of iron and thermal
 1010 evolution of the Earth’s core. *Physics of the Earth and Planetary Interiors*,
 1011 224(C), 88–103.
- 1012 Grand, S. P. (2002). Mantle shear-wave tomography and the fate of subducted
 1013 slabs. *Philosophical Transactions of the Royal Society of London Series a-*
 1014 *Mathematical Physical and Engineering Sciences*, 360(1800), 2475–2491.
- 1015 Grigné, C., Labrosse, S., & Tackley, P. J. (2007, August). Convection under a

- 1016 lid of finite conductivity in wide aspect ratio models: Effect of continents on
 1017 the wavelength of mantle flow. *Journal of Geophysical Research: Solid Earth*
 1018 (1978–2012), 112(B8).
- 1019 Guillou, L., & Jaupart, C. (1995, December). On the effect of continents on man-
 1020 tle convection. *Journal of Geophysical Research: Solid Earth (1978–2012)*,
 1021 100(B12), 24217–24238.
- 1022 Gurnis, M. (1988, April). Large-scale mantle convection and the aggregation and
 1023 dispersal of supercontinents. *Nature*, 332(6166), 695–699.
- 1024 Hawkesworth, C. J., & Kemp, A. I. S. (2006, October). Evolution of the continental
 1025 crust. *Nature*, 443(7113), 811–817.
- 1026 Haxby, W. F., & Weissel, J. K. (1986). Evidence for small-scale mantle convection
 1027 from Seasat altimeter data. *Journal of Geophysical Research*, 91(B3), 3507–
 1028 3520.
- 1029 Hernlund, J. W. (2010, June). On the interaction of the geotherm with a post-
 1030 perovskite phase transition in the deep mantle. *Physics of the Earth and Plan-
 1031 etary Interiors*, 180(3–4), 222–234.
- 1032 Hernlund, J. W., & Tackley, P. J. (2008, December). Modeling mantle convection in
 1033 the spherical annulus. *Physics of the Earth and Planetary Interiors*, 171(1–4),
 1034 48–54.
- 1035 Hernlund, J. W., Thomas, C., & Tackley, P. J. (2005, April). A doubling of the
 1036 post-perovskite phase boundary and structure of the Earth’s lowermost man-
 1037 tle. *Nature*, 434(7035), 882–886.
- 1038 Heron, P. J., & Lowman, J. P. (2010, November). Thermal response of the man-
 1039 tle following the formation of a “super-plate”. *Geophysical Research Letters*,
 1040 37(22).
- 1041 Heron, P. J., & Lowman, J. P. (2011, September). The effects of supercontinent size
 1042 and thermal insulation on the formation of mantle plumes. *Tectonophysics*,
 1043 510(1–2), 28–38.
- 1044 Heron, P. J., & Lowman, J. P. (2014, January). The impact of Rayleigh number on
 1045 assessing the significance of supercontinent insulation. *Journal of Geophysical*
 1046 *Research: Solid Earth*, 119(1), 711–733.
- 1047 Heron, P. J., Lowman, J. P., & Stein, C. (2015, May). Influences on the position-
 1048 ing of mantle plumes following supercontinent formation. *Journal of Geophysi-
 1049 cal Research: Solid Earth*, 120(5), 3628–3648.
- 1050 Herzberg, C., Raterron, P., & Zhang, J. (2000). New experimental observations
 1051 on the anhydrous solidus for peridotite KLB-1. *Geochemistry, Geophysics,*
 1052 *Geosystems*, 1(11), –n/a.
- 1053 Hirth, G., & Kohlstedt, D. L. (1996, October). Water in the oceanic upper mantle:
 1054 implications for rheology, melt extraction and the evolution of the lithosphere.
 1055 *Earth and Planetary Science Letters*, 144(1–2), 93–108.
- 1056 Hooper, P. R., Camp, V. E., Reidel, S. P., & Ross, M. E. (2007). The origin of the
 1057 Columbia River flood basalt province: Plume versus nonplume models. In *Spe-
 1058 cial paper 430: Plates, plumes and planetary processes* (pp. 635–668). Geologi-
 1059 cal Society of America.
- 1060 Houser, C., Masters, G., Shearer, P., & Laske, G. (2008, July). Shear and comp-
 1061 ressional velocity models of the mantle from cluster analysis of long-period
 1062 waveforms. *Geophysical Journal International*, 174(1), 195–212.
- 1063 Hunt, S. A., Weidner, D. J., Li, L., Wang, L., Walte, N. P., Brodholt, J. P., & Dob-
 1064 son, D. P. (2009, October). Weakening of calcium iridate during its trans-
 1065 formation from perovskite to post-perovskite. *Nature Geoscience*, 2(11),
 1066 794–797.
- 1067 Irifune, T., & Ringwood, A. E. (1993, May). Phase-Transformations in Subducted
 1068 Oceanic-Crust and Buoyancy Relationships at Depths of 600–800 Km in the
 1069 Mantle. *Earth and Planetary Science Letters*, 117(1–2), 101–110.
- 1070 Jayananda, M., Kano, T., Peucat, J. J., & Channabasappa, S. (2008, April). 3.35

- 1071 Ga komatiite volcanism in the western Dharwar craton, southern India: Con-
 1072 straints from Nd isotopes and whole-rock geochemistry. *Precambrian research*,
 1073 *162*(1-2), 160–179.
- 1074 Jordan, T. H. (1978). Composition and development of the continental tectosphere.
 1075 *Nature*, *274*(5671), 544–548.
- 1076 Jordan, T. H. (1979). Mineralogies, densities and seismic velocities of garnet lher-
 1077 zolites and their geophysical implications. In *The mantle sample: Inclusion in*
 1078 *kimberlites and other volcanics* (pp. 1–14). Washington, D. C.: American Geo-
 1079 physical Union.
- 1080 Karato, S. i., & Wu, P. (1993, May). Rheology of the Upper Mantle: A Synthesis.
 1081 *Science*, *260*(5109), 771–778.
- 1082 Kelemen, P. B., Hirth, G., Shimizu, N., Spiegelman, M., & Dick, H. J. (1997, Febru-
 1083 ary). A review of melt migration processes in the adiabatically upwelling man-
 1084 tle beneath oceanic spreading ridges. *Philosophical Transactions of the Royal*
 1085 *Society of London Series a-Mathematical Physical and Engineering Sciences*,
 1086 *355*(1723), 283–318.
- 1087 Lay, T., Hernlund, J., & Buffett, B. A. (2008). Core–mantle boundary heat flow.
 1088 *Nature Geoscience*, *1*(1), 25–32.
- 1089 Lay, T., Hernlund, J., Garnero, E. J., & Thorne, M. S. (2006). A post-perovskite
 1090 lens and D'' heat flux beneath the central Pacific. *Science*, *314*(5803), 1272–
 1091 1276.
- 1092 Lee, C.-T. A. (2003, September). Compositional variation of density and seismic
 1093 velocities in natural peridotites at STP conditions: Implications for seismic
 1094 imaging of compositional heterogeneities in the upper mantle. *Journal of*
 1095 *Geophysical Research*, *108*(B9), 589.
- 1096 Lenardic, A., & Moresi, L. (2001). Heat flow scaling for mantle convection below
 1097 a conducting lid: Resolving seemingly inconsistent modeling results regarding
 1098 continental heat flow. *Geophysical Research Letters*, *28*(7), 1311–1314.
- 1099 Lenardic, A., Moresi, L., Jellinek, A., & Manga, M. (2005, June). Continental in-
 1100 sulation, mantle cooling, and the surface area of oceans and continents. *Earth*
 1101 *and Planetary Science Letters*, *234*(3-4), 317–333.
- 1102 Lenardic, A., Moresi, L., Jellinek, A. M., O’Neill, C. J., Cooper, C. M., & Lee, C. T.
 1103 (2011, October). Continents, supercontinents, mantle thermal mixing, and
 1104 mantle thermal isolation: Theory, numerical simulations, and laboratory exper-
 1105 iments. *Geochemistry, Geophysics, Geosystems*, *12*(10).
- 1106 Leng, W., & Zhong, S. (2008). Controls on plume heat flux and plume excess tem-
 1107 perature. *Journal of Geophysical Research: Solid Earth*, *113*(B4).
- 1108 Li, X. D., & Romanowicz, B. (1996). Global mantle shear velocity model developed
 1109 using nonlinear asymptotic coupling theory. *Journal of Geophysical Research:*
 1110 *Solid Earth*, *101*(B10), 22245–22272.
- 1111 Lourenço, D. L., Rozel, A., & Tackley, P. J. (2016). Melting-induced crustal produc-
 1112 tion helps plate tectonics on Earth-like planets. *Earth and Planetary Science*
 1113 *Letters*, *439*, 18–28.
- 1114 Lowman, J. P., & Gable, C. W. (1999, September). Thermal evolution of the man-
 1115 tle following continental aggregation in 3D convection models. *Geophysical Re-*
 1116 *search Letters*, *26*(17), 2649–2652.
- 1117 Lowman, J. P., & Jarvis, G. T. (1993, October). Mantle convection flow reversals
 1118 due to continental collisions. *Geophysical Research Letters*, *20*(19), 2087–2090.
- 1119 Lowman, J. P., & Jarvis, G. T. (1996, November). Continental collisions in wide
 1120 aspect ratio and high Rayleigh number two-dimensional mantle convection
 1121 models. *Journal of Geophysical Research*, *101*(B11), 25485–25497.
- 1122 Marquart, G., Schmeling, H., & Braun, A. (1999, September). Small-scale instabil-
 1123 ities below the cooling oceanic lithosphere. *Geophysical Journal International*,
 1124 *138*(3), 655–666.
- 1125 Masters, G., Laske, G., Bolton, H., & Dziewonski, A. (2000). *The Relative Behavior*

- 1126 *of Shear Velocity, Bulk Sound Speed, and Compressional Velocity in the Man-*
 1127 *tle: Implications for Chemical and Thermal Structure* (Vol. 117). Washington,
 1128 D. C.: American Geophysical Union.
- 1129 McKenzie, D., & Bickle, M. J. (1988, June). The Volume and Composition of Melt
 1130 Generated by Extension of the Lithosphere. *Journal of Petrology*, 29(3), 625–
 1131 679.
- 1132 Mittelstaedt, E., & Tackley, P. J. (2006, January). Plume heat flow is much lower
 1133 than CMB heat flow. *Earth and Planetary Science Letters*, 241(1-2), 202–210.
- 1134 Mole, D. R., Fiorentini, M. L., Thébaud, N., Cassidy, K. F., McCuaig, T. C., Kirk-
 1135 land, C. L., ... Miller, J. (2014, July). Archean komatiite volcanism controlled
 1136 by the evolution of early continents. *Proceedings of the National Academy of*
 1137 *Sciences*, 111(28), 10083–10088.
- 1138 Moresi, L., & Solomatov, V. (1998). Mantle convection with a brittle lithosphere:
 1139 thoughts on the global tectonic styles of the earth and venus. *Geophysical*
 1140 *Journal International*, 133(3).
- 1141 Morgan, W. J. (1972). Plate Motions and Deep Mantle Convection. In R. Shagam et
 1142 al. (Eds.), *Studies in earth and space sciences*. Geological Society of America.
- 1143 Nakagawa, T., & Tackley, P. J. (2004, March). Effects of thermo-chemical mantle
 1144 convection on the thermal evolution of the Earth’s core. *Earth and Planetary*
 1145 *Science Letters*, 220(1-2), 107–119.
- 1146 Nakagawa, T., & Tackley, P. J. (2012). Influence of magmatism on mantle cooling,
 1147 surface heat flow and Urey ratio. *Earth and Planetary Science Letters*, 329, 1–
 1148 10.
- 1149 Nakagawa, T., Tackley, P. J., Deschamps, F., & Connolly, J. A. D. (2010, August).
 1150 Earth and Planetary Science Letters. *Earth and Planetary Science Letters*,
 1151 296(3-4), 403–412.
- 1152 Neal, C. R., Mahoney, J. J., Kroenke, L. W., Duncan, R. A., & Petterson, M. G.
 1153 (1997, January). The Ontong Java plateau. In *Large igneous provinces: Conti-*
 1154 *nenental, oceanic, and planetary flood volcanism* (pp. 183–216). Washington, D.
 1155 C.: American Geophysical Union.
- 1156 Nisbet, E. G. (1982). The tectonic setting and petrogenesis of komatiites. In
 1157 N. T. Arndt & E. G. Nisbet (Eds.), *Komatiites* (pp. 501–520). George Allen &
 1158 Unwin.
- 1159 Ogawa, M. (2014, March). Two-stage evolution of the Earth’s mantle inferred
 1160 from numerical simulation of coupled magmatism-mantle convection system
 1161 with tectonic plates. *Journal of Geophysical Research: Solid Earth*, 119(3),
 1162 2462–2486.
- 1163 O’Neill, C., Lenardic, A., Jellinek, A. M., & Moresi, L. (2009, June). Influence of su-
 1164 percontinents on deep mantle flow. *Gondwana Research*, 15(3-4), 276–287.
- 1165 Ono, S., Ito, E., & Katsura, T. (2001). Mineralogy of subducted basaltic crust
 1166 (MORB) from 25 to 37 GPa, and chemical heterogeneity of the lower mantle.
 1167 *Earth and Planetary Science Letters*, 190(1-2), 57–63.
- 1168 Panning, M., & Romanowicz, B. (2006, October). A three-dimensional radially
 1169 anisotropic model of shear velocity in the whole mantle. *Geophysical Journal*
 1170 *International*, 167(1), 361–379.
- 1171 Pearson, D. G., Parman, S. W., & Nowell, G. M. (2007). A link between large
 1172 mantle melting events and continent growth seen in osmium isotopes. *Nature*,
 1173 449(7159), 202–205.
- 1174 Phillips, B., & Bunge, H. (2005, April). Heterogeneity and time dependence in 3D
 1175 spherical mantle convection models with continental drift. *Earth and Planetary*
 1176 *Science Letters*, 233(1-2), 121–135.
- 1177 Phillips, B. R., & Coltice, N. (2010). Temperature beneath continents as a func-
 1178 tion of continental cover and convective wavelength. *Journal of Geophysical*
 1179 *Research*, 115(B4).
- 1180 Pollack, H. N. (1986, October). Cratonization and thermal evolution of the mantle.

- 1181 *Earth and Planetary Science Letters*, 80(1-2), 175–182.
- 1182 Pozzo, M., Davies, C., Gubbins, D., & Alfe, D. (2013, April). Thermal and electrical
1183 conductivity of iron at Earth’s core conditions. *Nature*, 485(7398), 355–358.
- 1184 Rampino, M. R., & Stothers, R. B. (1988, August). Flood Basalt Volcanism During
1185 the Past 250 Million Years. *Science*, 241(4866), 663–668.
- 1186 Ricard, Y., Richards, M., Lithgow-Bertelloni, C., & Le Stunff, Y. (1993). A geody-
1187 namic model of mantle density heterogeneity. *Journal of Geophysical Research*,
1188 98(B12), 21895–21909.
- 1189 Ricard, Y., Vigny, C., & Froidevaux, C. (1989, October). Mantle heterogeneities,
1190 geoid, and plate motion: A Monte Carlo inversion. *Journal of Geophysical Re-
1191 search*, 94(B10), 13739–13754.
- 1192 Richards, M. A., Duncan, R. A., & Courtillot, V. E. (1989, October). Flood Basalts
1193 and Hot-Spot Tracks: Plume Heads and Tails. *Science*, 246(4926), 103–107.
- 1194 Ritsema, J., Deuss, A., van Heijst, H. J., & Woodhouse, J. H. (2011, December).
1195 S40RTS: a degree-40 shear-velocity model for the mantle from new Rayleigh
1196 wave dispersion, teleseismic traveltime and normal-mode splitting function
1197 measurements. *Geophysical Journal International*, 184(3), 1223–1236.
- 1198 Ritsema, J., van Heijst, H. J., & Woodhouse, J. H. (1999). Complex shear wave ve-
1199 locity structure imaged beneath Africa and Iceland. *Science*, 286(5446), 1925–
1200 1928.
- 1201 Rolf, T., Coltice, N., & Tackley, P. J. (2012, October). Linking continental drift,
1202 plate tectonics and the thermal state of the Earth’s mantle. *Earth and Plane-
1203 tary Science Letters*, 351-352(C), 134–146.
- 1204 Rolf, T., & Tackley, P. J. (2011, September). Focussing of stress by continents in
1205 3D spherical mantle convection with self-consistent plate tectonics. *Geophysical
1206 Research Letters*, 38(18).
- 1207 Rozel, A. B., Golabek, G. J., Jain, C., Tackley, P. J., & Gerya, T. (2017, May).
1208 Continental crust formation on early Earth controlled by intrusive magmatism.
1209 *Nature*, 545(7654), 332–335.
- 1210 Rudnick, R. L., & Gao, S. (2003). Composition of the Continental Crust. In *Treatise
1211 on geochemistry* (pp. 1–64). Elsevier.
- 1212 Schubert, G., Turcotte, D. L., & Olson, P. (2001). *Mantle Convection in the Earth
1213 and Planets*. Cambridge: Cambridge University Press.
- 1214 Schutt, D. L., & Leshner, C. E. (2006, May). Effects of melt depletion on the density
1215 and seismic velocity of garnet and spinel lherzolite. *Journal of Geophysical Re-
1216 search*, 111(B5).
- 1217 Scrutton, R. A. (1973). The age relationship of igneous activity and continental
1218 break-up. *Geological Magazine*, 110(03), 227–234.
- 1219 Sengör, A. M. C., & Burke, K. (1978, January). Relative timing of rifting and vol-
1220 canism on Earth and its tectonic implications. *Geophysical Research Letters*,
1221 5(6), 419–421.
- 1222 Solomatov, V. S. (1995, February). Scaling of Temperature-Dependent and Stress-
1223 Dependent Viscosity Convection. *Physics of Fluids*, 7(2), 266–274.
- 1224 Stevenson, D. J. (1990). Fluid dynamics of core formation. In *Origin of the earth
1225* (pp. 231–249). New York: Oxford University Press.
- 1226 Su, W. J., & Dziewonski, A. M. (1997, March). Simultaneous inversion for 3-D vari-
1227 ations in shear and bulk velocity in the mantle. *Physics of the Earth and Plan-
1228 etary Interiors*, 100(1-4), 135–156.
- 1229 Su, W. J., Woodward, R. L., & Dziewonski, A. M. (1994). Degree-12 Model of Shear
1230 Velocity Heterogeneity in the Mantle. *Journal of Geophysical Research: Solid
1231 Earth*, 99(B4), 6945–6980.
- 1232 Tackley, P. J. (2008a, December). Modelling compressible mantle convection with
1233 large viscosity contrasts in a three-dimensional spherical shell using the yin-
1234 yang grid. *Physics of the Earth and Planetary Interiors*, 171(1-4), 7–18.
- 1235 Tackley, P. J. (2008b, November). Self-consistent generation of tectonic plates in

- 1236 time-dependent, three-dimensional mantle convection simulations. *Geochem-*
 1237 *istry, Geophysics, Geosystems*, 1(8).
- 1238 Tackley, P. J., Ammann, M., Brodholt, J. P., Dobson, D. P., & Valencia, D. (2013,
 1239 July). Mantle dynamics in super-Earths: Post-perovskite rheology and self-
 1240 regulation of viscosity. *Icarus*, 225(1), 50–61.
- 1241 Tackley, P. J., & King, S. D. (2003, April). Testing the tracer ratio method for mod-
 1242 eling active compositional fields in mantle convection simulations. *Geochem-*
 1243 *istry, Geophysics, Geosystems*, 4(4).
- 1244 van der Hilst, R. D., de Hoop, M. V., Wang, P., Shim, S. H., Ma, P., & Tenorio,
 1245 L. (2007, March). Seismostratigraphy and Thermal Structure of Earth’s
 1246 Core-Mantle Boundary Region. *Science*, 315(5820), 1813–1817.
- 1247 van der Hilst, R. D., Widiyantoro, S., & Engdahl, E. R. (1997, April). Evidence for
 1248 deep mantle circulation from global tomography. *Nature*, 386(6625), 578–584.
- 1249 Wang, Q., Schi tte, L., & Campbell, I. H. (1996, August). Geochronological con-
 1250 straints on the age of komatiites and nickel mineralisation in the Lake John-
 1251 ston greenstone belt, Yilgarn Craton, Western Australia. *Australian Journal of*
 1252 *Earth Sciences*, 43(4), 381–385.
- 1253 White, R., & McKenzie, D. (1989). Magmatism at rift zones: The generation of vol-
 1254 canic continental margins and flood basalts. *Journal of Geophysical Research*,
 1255 94(B6), 7685–7729.
- 1256 Wooden, J. L., Czamanske, G. K., Fedorenko, V. A., Arndt, N. T., Chauvel, C.,
 1257 Bouse, R. M., . . . Siems, D. F. (1993, August). Isotopic and trace-element
 1258 constraints on mantle and crustal contributions to Siberian continental flood
 1259 basalts, Noril’sk area, Siberia. *GEOCHIMICA ET COSMOCHIMICA ACTA*,
 1260 57(15), 3677–3704.
- 1261 Xie, S., & Tackley, P. J. (2004a, September). Evolution of helium and argon isotopes
 1262 in a convecting mantle. *Physics of the Earth and Planetary Interiors*, 146(3-
 1263 4), 417–439.
- 1264 Xie, S., & Tackley, P. J. (2004b, November). Evolution of U-Pb and Sm-Nd systems
 1265 in numerical models of mantle convection and plate tectonics. *Journal of Geo-*
 1266 *physical Research*, 109(B11).
- 1267 Xu, W., Lithgow-Bertelloni, C., Stixrude, L., & Ritsema, J. (2008, October). The
 1268 effect of bulk composition and temperature on mantle seismic structure. *Earth*
 1269 *and Planetary Science Letters*, 275(1-2), 70–79.
- 1270 Yamazaki, D., & Karato, S.-i. (2001, April). Some mineral physics constraints on the
 1271 rheology and geothermal structure of Earth’s lower mantle. *American Mineral-*
 1272 *ogist*, 86(4), 385–391.
- 1273 Yoshida, M., Iwase, Y., & Honda, S. (1999, April). Generation of plumes under
 1274 a localized high viscosity lid in 3-D spherical shell convection. *Geophysical Re-*
 1275 *search Letters*, 26(7), 947–950.
- 1276 Zerr, A., Diegeler, A., & Boehler, R. (1998, July). Solidus of Earth’s deep mantle.
 1277 *Science*, 281(5374), 243–246.
- 1278 Zhang, P., Cohen, R. E., & Haule, K. (2015, January). Effects of electron corre-
 1279 lations on transport properties of iron at Earth’s core conditions. *Nature*,
 1280 517(7536), 605–607.
- 1281 Zhao, D. P. (2004). Global tomographic images of mantle plumes and subduct-
 1282 ing slabs: insight into deep Earth dynamics. *Physics of the Earth and Plane-*
 1283 *tary Interiors*, 146(1-2), 3–34.
- 1284 Zhong, S., & Gurnis, M. (1993, July). Dynamic feedback between a continentlike
 1285 raft and thermal convection. *Journal of Geophysical Research*, 98(B7), 12219–
 1286 12232.
- 1287 Zhong, S., & Liu, X. (2016, January). The long-wavelength mantle structure
 1288 and dynamics and implications for large-scale tectonics and volcanism in the
 1289 Phanerozoic. *Gondwana Research*, 29(1), 83–104.
- 1290 Zhong, S., Zhang, N., Li, Z.-X., & Roberts, J. H. (2007). Supercontinent cycles, true

1291 polar wander, and very long-wavelength mantle convection. *Earth and Plane-*
1292 *tary Science Letters*, 261(3-4), 551–564.
1293 Zhong, S. J. (2006). Constraints on thermochemical convection of the mantle from
1294 plume heat flux, plume excess temperature, and upper mantle temperature.
1295 *Journal of Geophysical Research: Solid Earth*, 111(B4).